

A complete electronic version of this article and other services, including high-resolution figures, can be found at:

<http://stm.sciencemag.org/content/2/42/42ra54.full.html>

Supporting Online Material can be found at:

"Supplementary Material"

<http://stm.sciencemag.org/content/suppl/2010/07/27/2.42.42ra54.DC1.html>

This article cites 134 articles, 44 of which can be accessed free:

<http://stm.sciencemag.org/content/2/42/42ra54.full.html#ref-list-1>

Information about obtaining reprints of this article or about obtaining permission to reproduce this article in whole or in part can be found at:

<http://www.sciencemag.org/about/permissions.dtl>

MUSCULAR DYSTROPHY

A Human-Specific Deletion in Mouse *Cmah* Increases Disease Severity in the mdx Model of Duchenne Muscular Dystrophy

Kumaran Chandrasekharan,¹ Jung Hae Yoon,¹ Ying Xu,² Sarah deVries,¹ Marybeth Camboni,¹ Paulus M. L. Janssen,² Ajit Varki,³ Paul T. Martin^{1,2,4*}

(Published 28 July 2010; Volume 2 Issue 42 42ra54)

During the evolution of humans, an inactivating deletion was introduced in the *CMAH* (cytidine monophosphate-sialic acid hydroxylase) gene, which eliminated biosynthesis of the common mammalian sialic acid *N*-glycolylneuraminic acid from all human cells. We found that this human-specific change in sialylation capacity contributes to the marked discrepancy in phenotype between the mdx mouse model for Duchenne muscular dystrophy (DMD) and the human disease. When compared to human patients with DMD, mdx mice show reduced severity or slower development of clinically relevant disease phenotypes, despite lacking dystrophin protein in almost all muscle cells. This is especially true for the loss of ambulation, cardiac and respiratory muscle weakness, and decreased life span, all of which are major phenotypes contributing to DMD morbidity and mortality. These phenotypes occur at an earlier age or to a greater degree in mdx mice that also carry a human-like mutation in the mouse *Cmah* gene, possibly as a result of reduced strength and expression of the dystrophin-associated glycoprotein complex and increased activation of complement. *Cmah*-deficient mdx mice are a small-animal model for DMD that better approximates the human glycome and its contributions to muscular dystrophy.

INTRODUCTION

Duchenne muscular dystrophy (DMD) is a severe, progressive disease of muscle wasting that results from X-linked recessive mutations or deletions in the dystrophin gene that cause loss of dystrophin protein (1, 2). DMD occurs in ~1 of every 3500 boys (3). Boys with DMD can have evidence of muscle damage at birth (such as increased serum creatine kinase) but are usually diagnosed after showing delayed motor development milestones at age 2 to 5 years (4). Muscle wasting, the replacement of muscle tissue with fat or extracellular matrix (ECM), progresses with age, leading to severe muscle weakness and lack of ambulation, typically by age 12 (5). Children most often perish from the disease as a result of complications related to cardiac or respiratory failure in the second to third decade of life (4). Although high-dose corticosteroids can preserve ambulation for several years in younger DMD patients (6, 7), no available therapy changes the ultimate course of the disease, even though the gene defects responsible for DMD have been known for more than 20 years (1, 2).

The mdx mouse (8), the most commonly used animal model for DMD (1, 2, 9–11), carries a point mutation in exon 23 of the dystrophin gene that leads to a premature stop codon, resulting in the absence of dystrophin protein in almost all skeletal and cardiac muscle cells (9), just as in DMD (1). Loss of dystrophin in mdx mouse and DMD muscles disrupts the dystrophin-associated glycoprotein (DAG) complex, proteins that link the basal lamina of the ECM that sur-

rounds every skeletal myofiber through the sarcolemmal membrane to the F-actin cytoskeleton (12–16). Consistent with their central role in disease, loss-of-function mutations in almost all DAG proteins cause forms of muscular dystrophy (4, 17–20). Mutations in laminin $\alpha 2$ (*LAMA2*), the principal laminin in the muscle basal lamina (21, 22), cause congenital muscular dystrophy 1A (MDC1A); mutations in *POMT1*, *POMT2*, *POMGnT1*, *FKTN*, *FKRP*, or *LARGE*, genes that affect the glycosylation of α -dystroglycan (α DG) (23), an extracellular membrane-associated protein that binds laminins in a glycosylation-dependent manner (16, 24), cause congenital or limb-girdle muscular dystrophies (Walker-Warburg syndrome, muscle-eye-brain disease, Fukuyama congenital muscular dystrophy, MDC1C, MDC1D, LGMD2I, LGMD2K, and LGMD2L-N); and mutations in α -, β -, γ -, and δ -sarcoglycans (*SGCA*, *SGCB*, *SGCG*, and *SGCD*), all DAG transmembrane proteins, cause forms of limb-girdle muscular dystrophy (LGMD2D, LGMD2E, LGMD2C, and LGMD2F, respectively). In DMD and mdx muscle, dystroglycan, sarcoglycans, and other DAG proteins are reduced in concentration (12, 15, 25, 26), whereas utrophin, an autosomal paralog of dystrophin (27) that can bind many of the same proteins as dystrophin (28–30), is up-regulated and can ameliorate disease (31, 32).

Although mdx mice display a number of aspects of DMD disease biology that make them useful for translational studies, the progression and severity of muscular dystrophy in mdx mice does not completely parallel the human disease. Muscle damage and concomitant muscle regeneration are present at 3 to 4 weeks of age in mdx animals, and such skeletal muscle pathology progresses, along with variable muscle weakness, in extent and severity as the animals mature (33, 34). Muscle damage correlates with deficits in the physiological properties of mdx skeletal myofibers, including increased damage in response to eccentric contractions (35–38), reduced muscle specific force (35, 36, 38–41), increased calcium leakage into myofibers (42, 43), increased dye uptake into myofibers (36, 38, 44), and increased release of muscle enzymes

¹Center for Gene Therapy, Research Institute at Nationwide Children's Hospital, 700 Children's Drive, Columbus, OH 43205, USA. ²Department of Physiology and Cell Biology, Ohio State University College of Medicine, Columbus, OH 43210, USA. ³Departments of Medicine and Cellular and Molecular Medicine, University of California, San Diego, La Jolla, CA 92093, USA. ⁴Department of Pediatrics, Ohio State University College of Medicine, Columbus, OH 43205, USA.

*To whom correspondence should be addressed. E-mail: paul.martin@nationwidechildrens.org

into the serum (45, 46). Many of these characteristics are exacerbated by a regimen of forced exercise (47–49). Replacement of muscle tissue with ECM or fat (muscle wasting), the process that ultimately drives muscle weakness in DMD, becomes significant in the diaphragm at 6 months of age (40). Thus, wasting of the diaphragm muscle in mdx mice phenocopies the wasting that occurs in many muscles in patients with DMD. Most large mdx limb muscles, however, only show significant fibrosis at very old ages (50, 51).

Evidence of physiological decrements in cardiac muscle is also present at 10 months of age in mdx mice (52), but, as with most skeletal muscles, fibrotic changes in the heart are far more evident in very old animals [for example, 20 months (51)]. Older animals also show other evidence of cardiac pathology, including necrotic lesions and cardiomyopathy, and have a ~20% reduction in life span relative to normal wild-type mice (10, 53, 54). The disease phenotypes that develop in mdx mice have allowed them to be used to great effect to demonstrate proof of principle for many therapeutic approaches, including gene replacement therapy (55–58), surrogate gene therapy (69–72), RNA splicing (73, 74), stop codon readthrough (75, 76), myoblast transfer (77–79), stem cell therapy (80–82), and various drug or nutritional therapies (83–85). All such studies, however, must be interpreted with the view that a number of the phenotypes most relevant to DMD morbidity and mortality—respiratory and cardiac muscle weakness and failure, loss of ambulation, and loss of life span—either are less severe or show delayed onset relative to the life span of a normal mouse when compared to the human disease.

Because the lack of these early-onset phenotypes in mdx mice does not pertain to loss of dystrophin, which is largely absent in mdx muscles, it is likely that other human-mouse genetic differences account for the differences in disease presentation. Although some have attributed the distinct times of onset to differences in size between mice and humans, mdx mice can manifest more severe dystrophic phenotypes when engineered to contain additional gene mutations [for example, mutations in utrophin (*mdxUtrn*^{-/-}) (86), integrin $\alpha 7$ (*mdxItga7*^{-/-}) (87), α -dystrobrevin (*mdxAdbn*^{-/-}) (88), or MyoD (*mdxMyod1*^{-/-}) (89)]. Unfortunately, none of these engineered mice better represent the human disease because all of these genes are expressed in DMD muscles (90–92). Although human-mouse differences in phe-

notype undoubtedly arise from multiple genetic differences, we chose to examine the contribution of glycans present on the cell surface, an aspect of molecular evolution that can be highly variable between mammalian species.

All glycoproteins and glycolipids within the plasma membrane contribute to the expression of a glycocalyx, a highly concentrated halo of carbohydrates (glycans) that surrounds the extracellular surface of all

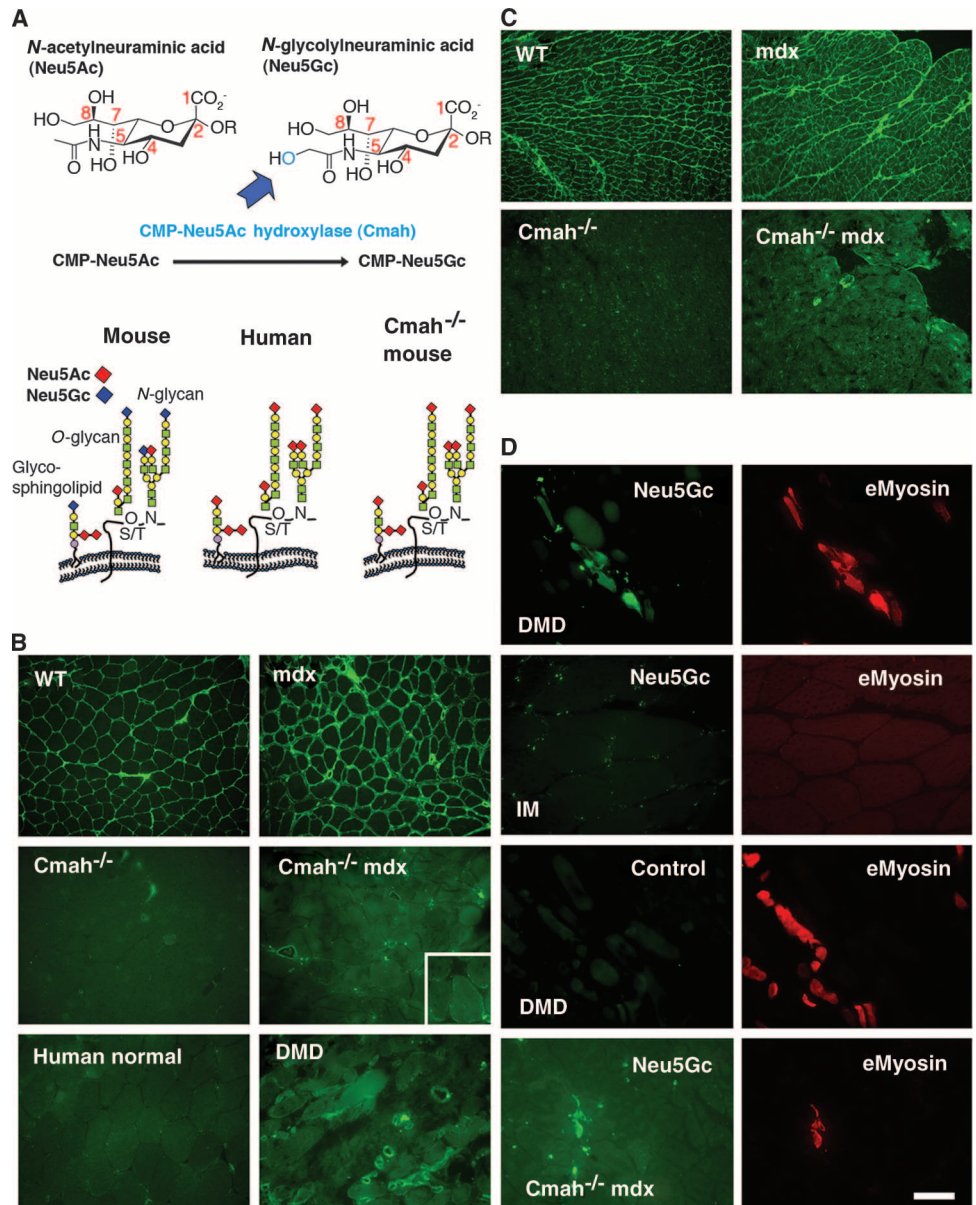


Fig. 1. Expression of Neu5Gc in normal and dystrophic mouse and human muscles. **(A)** Neu5Gc differs from Neu5Ac by an additional oxygen at the 5 position of this sialic acid [modified from (112)]. Because mice express a functional *Cmah* gene, they incorporate sialic acids at the outer ends of glycolipids and glycoproteins that are usually either Neu5Gc or Neu5Ac. Humans and *Cmah*^{-/-} mice, by contrast, contain an inactivating deletion in *Cmah* and therefore do not express Neu5Gc on the surface of glycoconjugates but instead have increased Neu5Ac. **(B and C)** Skeletal muscles (B) and cardiac muscles (C) were immunostained with a Neu5Gc-specific antibody. **(D)** DMD and *Cmah*^{-/-} mdx skeletal muscles were costained for Neu5Gc (green) and embryonic myosin (eMyosin) (red), which marks regenerating myofibers or myoblasts. Scale bar, 100 μ m (B), 200 μ m (C), 50 μ m (D). IM, inflammatory myopathy (inclusion body myositis).

cells. Changes in the glycan repertoire could alter the biology of many systems and disease processes. Because infectious agents such as viruses and bacteria often use host cell glycans as receptors, cell surface glycans are also prone to alteration during natural selection, amplifying interspecies glycan differences (93).

Sialic acids, an important class of monosaccharides expressed on the terminal ends of glycan structures on many glycoproteins and glycolipids (94) that can take dozens of possible forms, are usually represented in most mammals by *N*-acetylneuraminic acid (Neu5Ac) and *N*-glycolylneuraminic acid (Neu5Gc). Neu5Gc differs from Neu5Ac by having an additional oxygen atom at the 5-*N*-acyl position (Fig. 1A). Neu5Gc expression requires the *CMAH* (cytidine monophosphate-sialic acid hydroxylase) gene, which encodes the cytidine 5'-monophosphate (CMP)-Neu5Ac hydroxylase, an enzyme that hydroxylates the 5-*N*-acetyl group of Neu5Ac on CMP-Neu5Ac to make CMP-Neu5Gc (95, 96). Both CMP-Neu5Ac and CMP-Neu5Gc are sugar nucleotide donors used by some 20 mammalian sialyltransferases to incorporate these sialic acids into glycans on proteins and lipids. Because most mammals, including mice, express a functional *CMAH* gene (Fig. 1A) (95, 96), they typically express a 50:50 mixture of Neu5Gc and Neu5Ac on glycoproteins and glycolipids in skeletal and cardiac muscles—the two cell types most affected in DMD. Dogs, for which there are human-like DMD models (10, 97, 98), contain almost undetectable Neu5Gc in skeletal muscle [2% of sialic acids on muscle gangliosides (99)], and humans express no Neu5Gc and instead have an excess of Neu5Ac (100). The altered sialic acid expression is due to the presence of an inactivating deletion in human *CMAH* that occurred about 2 million to 3 million years ago (101). All humans are null for Neu5Gc biosynthesis, and human cells should be devoid of Neu5Gc expression (93), although pathological human cells, such as cancer cells, can incorporate Neu5Gc from dietary sources via a salvage pathway and express Neu5Gc on their cell surface (100, 102). Because all humans also produce antibodies that recognize Neu5Gc (103, 104) as a foreign antigen, this incorporation creates Neu5Gc glycan “xeno-autoantigens,” which can alter cancer progression (105) and also

allows toxins that recognize Neu5Gc to affect humans (106). Because glycosylation can modify disease in mdx mice (46) and in other mouse models of muscular dystrophy (107, 108), we tested whether the *Cmah*

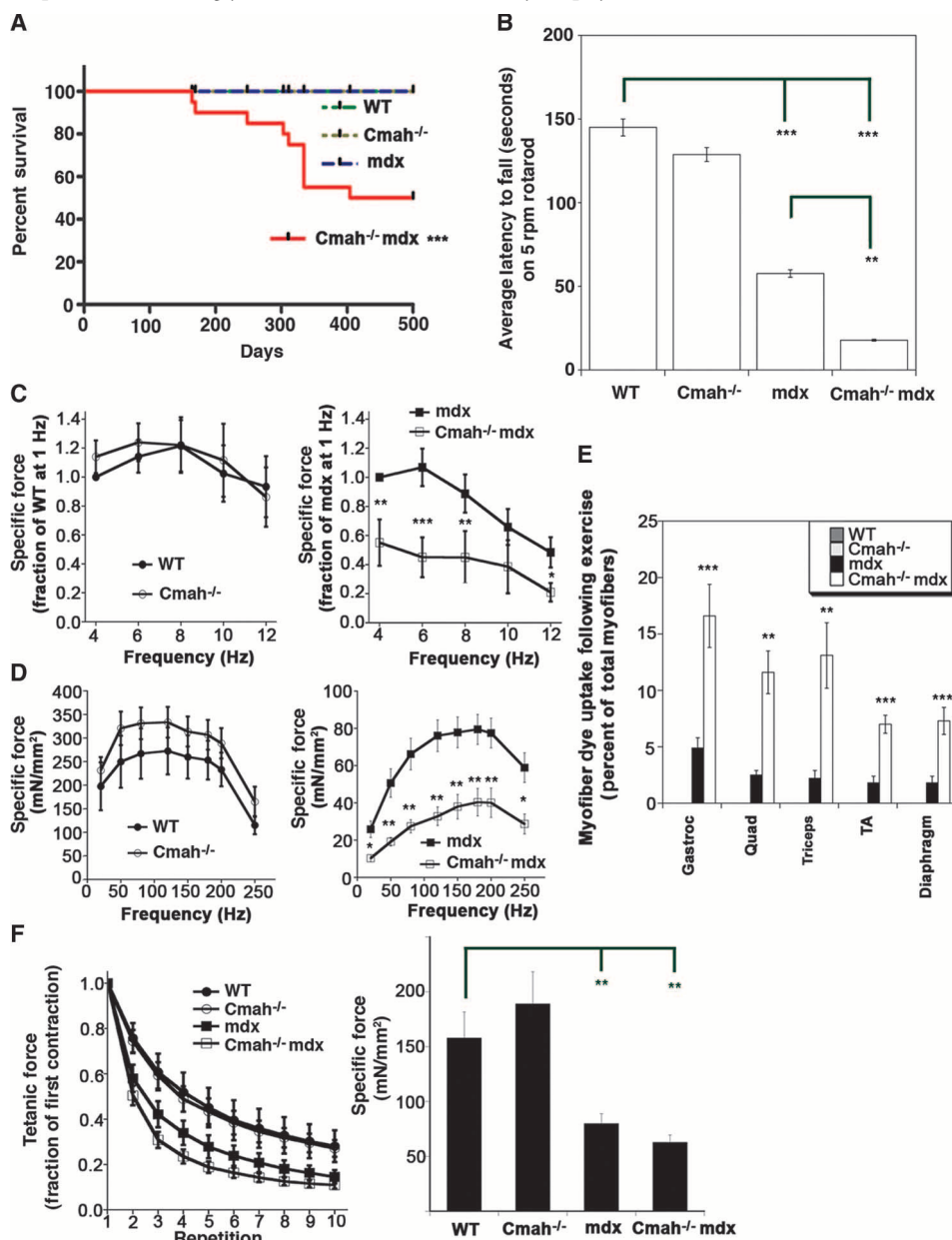


Fig. 2. Increased mortality and functional deficits in *Cmah*^{-/-}mdx skeletal and cardiac muscle. **(A)** *Cmah*^{-/-}mdx mice showed a highly significant decrease in life span relative to mdx, *Cmah*^{-/-}, and wild-type (WT) mice ($P < 0.001$ for *Cmah*^{-/-}mdx versus all others). **(B)** By 8 months of age, *Cmah*^{-/-}mdx showed a 70% reduction in time able to walk on a constant speed rotarod for 5 min relative to mdx littermates ($P < 0.001$), whereas *Cmah*^{-/-} mice did not show a significant decrease relative to WT ($P > 0.05$). **(C)** Developed tension (specific force in millinewtons per square millimeter) of isolated cardiac trabeculae muscles was reduced in 8-month-old *Cmah*^{-/-}mdx relative to mdx mice. **(D)** Specific force of diaphragm muscle was reduced in 8-month-old *Cmah*^{-/-}mdx animals relative to mdx. **(E)** EBD uptake into myofibers was increased after exercise in the gastrocnemius (Gastroc), quadriceps (Quad), tibialis anterior (TA), triceps, and diaphragm muscles of 2-month-old *Cmah*^{-/-}mdx mice relative to mdx. *Cmah*^{-/-} and WT muscles showed no dye uptake in any muscle. **(F)** Normalized specific force during repeated eccentric contractions (left) in the EDL muscle was reduced in *Cmah*^{-/-}mdx relative to mdx, as was maximal specific force. Error bars are SEM for $n = 75$ to 100 animals per condition in (A), 12 to 25 in (B), 5 to 9 in (C), 3 to 6 in (D), 5 to 6 in (E), and 11 to 12 in (F). * $P < 0.05$, ** $P < 0.01$, *** $P < 0.001$.

gene affects disease biology by introducing a human-like inactivating *Cmah* gene deletion into mdx mice. In doing so, we have developed a more genetically appropriate small-animal disease model for DMD that also has advantages for translational research.

RESULTS

Neu5Gc in *Cmah*-deficient mdx mice and in humans with DMD

To assess the role of *CMAH* in muscle disease, we incorporated a human-like inactivating deletion into the mouse *Cmah* gene (109) and bred it into the mdx mouse model for DMD for more than 15 generations, creating *Cmah*^{-/-}mdx mice on the same genetic background as mdx mice. To assess Neu5Gc production, we used an affinity-purified, Neu5Gc-specific immunoglobulin Y (IgY) polyclonal antibody from chickens (110), a species with no detectable Neu5Gc (110), to immunostain normal and diseased mouse and human muscle (Fig. 1, B to D). *Cmah*^{-/-} mice exhibited no Neu5Gc in skeletal or cardiac muscle tissue (Fig. 1, B and C), although occasional staining could be seen in blood vessels, as described previously (109). This staining results from small amounts of Neu5Gc incorporation into endothelial cells and can be avoided by feeding the mice a diet devoid of Neu5Gc (109). As expected, both wild-type and mdx mice had easily detectable Neu5Gc on the surface of both skeletal (Fig. 1B) and cardiac (Fig. 1C) muscle because mice normally express *Cmah* in these tissues. In all cases, staining with nonimmune chicken IgY gave no detectable staining of myofibers but did show occasional staining of mononucleated cells (fig. S1A). In addition, small regenerating muscles in mdx tissue showed higher Neu5Gc concentrations than did mature myofibers, even in *Cmah*^{+/-}mdx muscles (fig. S1B). As in *Cmah*^{-/-} mice, most skeletal myofibers in mice deficient for both *Cmah* and dystrophin (*Cmah*^{-/-}mdx) showed no Neu5Gc (fig. S1B). However, a small number (<1%) of myofibers in *Cmah*^{-/-}mdx muscles were strongly Neu5Gc-positive (Fig. 1B), as were some *Cmah*^{-/-}mdx cardiomyocytes (Fig. 1C). Some Neu5Gc-positive fibers in *Cmah*^{-/-}mdx skeletal muscles appeared to be undergoing necrosis because they lacked complete cytoplasm, but others appeared as normal regenerating myofibers or myoblasts (Fig. 1, B and D). Likewise, normal human skeletal muscle expressed no detectable Neu5Gc, but small regenerating and necrotic muscles from DMD patients showed easily detectable expression of Neu5Gc on the sarcolemmal membrane (Fig. 1B). Regenerating myofibers (and/or myoblasts) were identified in DMD and *Cmah*^{-/-}mdx skeletal muscle by costaining with embryonic myosin and were Neu5Gc-positive at a very early stage of development (Fig. 1D), often before expression of laminin α 2 (fig. S1C). Biopsies from patients with inflammatory myopathy (inclusion body myositis), in contrast to those from DMD patients, showed no Neu5Gc staining of myofibers (Fig. 1D). All muscles studied showed no gross deficit in overall sialic acid content, as evidenced by staining with lectins such as *Maackia amurensis* agglutinin (MAA), which bind both Neu5Ac and Neu5Gc (fig. S1, D and E). This assay could not detect the trace amounts of Neu5Gc in *Cmah*^{-/-}mdx muscles seen by the antibodies (Fig. 1, B to D), but this is not surprising because of the focal Neu5Gc staining pattern and the likely low Neu5Gc incorporation into muscle cells.

Accelerated disease onset and increased disease severity in *Cmah*^{-/-}mdx mice

The muscle histopathology of the mdx mouse is consistent with what is observed in DMD, yet many major phenotypic milestones of the clinical

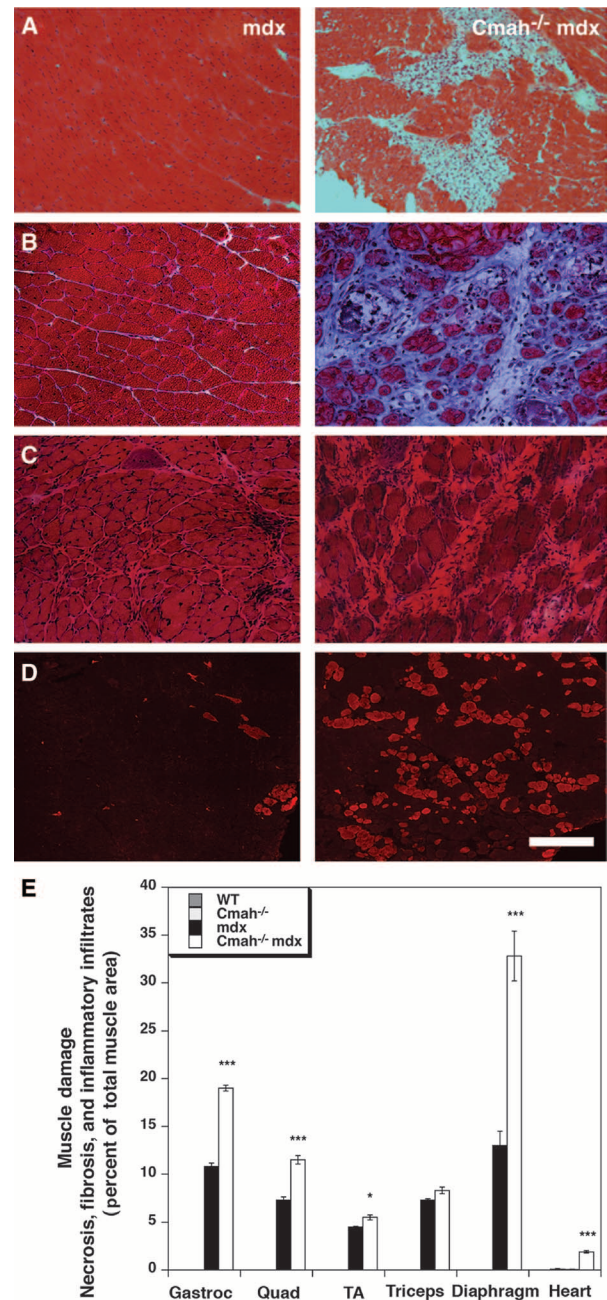
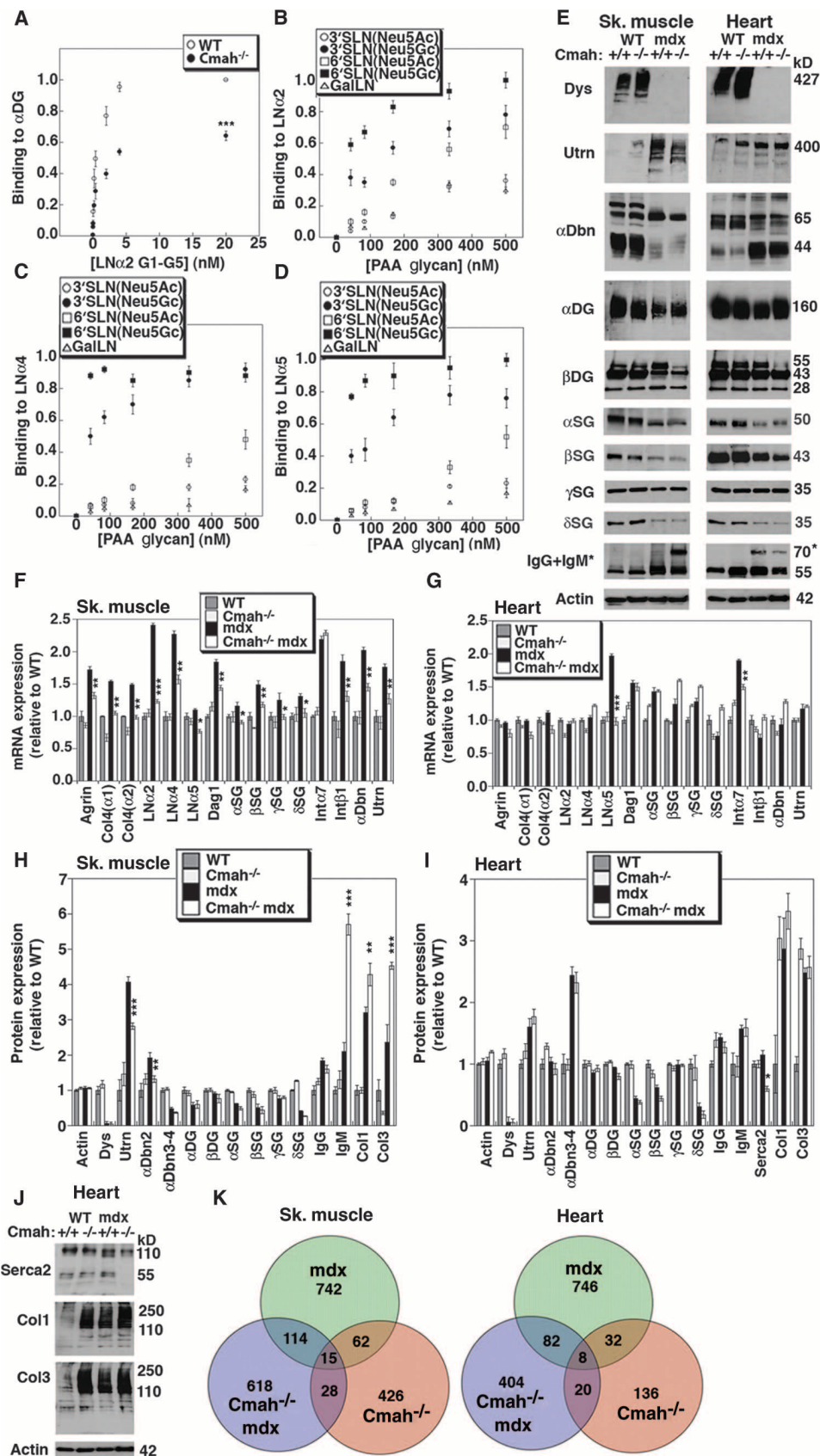


Fig. 3. Increased histopathology in *Cmah*^{-/-}mdx skeletal and cardiac muscle. (A) Three-month-old heart sections were stained with hematoxylin and eosin. *Cmah*^{-/-}mdx heart muscle had large mononuclear infiltrates normally not seen in age-matched mdx heart muscle. (B) Two-month-old mdx and *Cmah*^{-/-}mdx skeletal muscle (quadriceps) was stained with modified Mason's trichrome. Fibrosis, replacement of muscle tissue with collagen (blue), was evident in some regions of the *Cmah*^{-/-}mdx quadriceps muscle, whereas it was never observed in mdx muscle at this age. (C) Six-month-old diaphragm muscle was stained with hematoxylin and eosin. *Cmah*^{-/-}mdx diaphragm showed increased fibrosis relative to mdx. (D) EBD uptake in 2-month-old quadriceps muscle was increased, after exercise, in *Cmah*^{-/-}mdx muscle relative to mdx. (E) Areas of muscle damage were quantified for skeletal and heart muscles. No significant damage was measured in any WT or *Cmah*^{-/-} muscle. Scale bar, 200 μ m [(A), (B), and (D)], 100 μ m (C). Error bars are SEM for $n = 6$ to 12 per condition in (E).

Fig. 4. Molecular changes resulting from loss of Neu5Gc expression. **(A)** Loss of Neu5Gc (*Cmah*^{-/-}) on α DG led to decreased laminin α 2 (LN α 2) binding ($P < 0.001$ for WT versus *Cmah*^{-/-} at 20 nM). Affinity-purified recombinant G1 to G5 domain of laminin α 2 was used as the ligand. **(B to D)** Neu5Gc(α 2-3 or α 2-6)Gal β 1-4GlcNAc (3'SLN or 6'SLN)-biotin-PAA (PAA glycan) had significantly higher binding to laminin α 2 (B), laminin α 4 (C), and laminin α 5 (D) than did Neu5Ac(α 2-3 or α 2-6)Gal β 1-4GlcNAc-biotin-PAA ($P < 0.001$ for Neu5Gc versus Neu5Ac for all α 2-3 or α 2-6 sialic acid-linked comparisons at 500 nM). Gal α 1-3Gal β 1-4GlcNAc (GalLN)-PAA, by contrast, showed only very weak binding to laminins. **(E)** Immunoblot analysis of DAG protein changes in skeletal (Sk.) muscle and heart. Expected molecular masses (in kilodaltons) for proteins are as follows: dystrophin (Dys), 427; utrophin (Utrn), 400; α -dystrobrevin (α Dbn), 2, 65; α -dystrobrevins 3 and 4, 44; α DG, 160; β -dystroglycan (β DG), 43; α -sarcoglycan (α SG), 50; β -sarcoglycan (β SG), 43; γ -sarcoglycan (γ SG), 35; δ -sarcoglycan (δ SG), 35; mouse IgG, 55; mouse IgM*, 70; and actin, 42. **(F and G)** Gene expression changes in skeletal muscle and heart at 5 months of age. Col4(α 1), collagen IV, α 1 chain; Col4(α 2), collagen IV, α 2 chain; Dag1, dystroglycan 1; Int α 7, integrin α 7; Int β 1, integrin β 1. **(H and I)** Protein expression was quantified by densitometric scanning of Western blots in skeletal muscle or heart. Col1, collagen I; Col3, collagen III. **(J)** Western blots of heart muscle protein show increased collagen I and III expression in *Cmah*^{-/-}, mdx, and *Cmah*^{-/-}mdx cardiac muscle and reduced Serca2 in *Cmah*^{-/-}mdx muscle. Expected molecular masses (in kilodaltons) are as follows: collagen 1 (precursor), 140 to 210; collagen 3, 110 to 140; and Serca2, 100. **(K)** Two-month-old heart or skeletal muscle (gastrocnemius) mRNA was compared with microarrays ($n = 3$ per condition). Genes that were significantly up- or down-regulated by a factor of 2 or more ($P < 0.05$ between *Cmah*^{-/-}, mdx, or *Cmah*^{-/-}mdx and WT) were identified and subdivided according to whether they overlapped between groups. Error bars are SEM for $n = 6$ to 8 per condition in (A) to (D) and $n = 9$ to 10 in (F) to (I).



disease, including early loss of muscle tissue (wasting) and respiratory and cardiac failure, do not often appear until the animals are near the end of their normal life span (10, 11). As a likely consequence, life span is reduced in mdx mice by <20% when compared to wild-type controls (54). *Cmah*^{-/-}mdx mice, in contrast to mdx animals, showed a clinical progression and physiologic decrements more representative of what is seen in DMD patients, indicating that *Cmah* is a genetic modifier of disease in mdx mice (Fig. 2). *Cmah*^{-/-}mdx mice showed significant decreases in life span relative to mdx mice, with almost half of all animals dying by 11 months of age (Fig. 2A). At 8 months of age, most aged *Cmah*^{-/-}mdx mice showed impaired ambulation, with a 70% decrease on a constant speed (5 rpm) rotarod test as compared to mdx littermates (Fig. 2B). Although mdx mice are also impaired in ambulation at this age, *Cmah*^{-/-}mdx mice are impaired to a much greater extent. In DMD, the failure of diaphragm and cardiac muscles contributes the most to mortality. Aged (8-month-old) *Cmah*^{-/-}mdx mice showed significant deficits in diaphragm (Fig. 2C) and cardiac (Fig. 2D) muscle strength (specific force, defined as force normalized to muscle weight) relative to age-matched mdx controls. *Cmah*^{-/-}mdx diaphragm showed a reduction of 88% in peak force (at 125 Hz), and cardiac trabeculae of 60% (at 6 Hz), relative to the wild type (Fig. 2, C and D). mdx diaphragm also showed reduced specific force relative to the wild type, consistent with the fact that the diaphragm is the one muscle in mdx animals that shows significant fibrosis beyond 6 months of age (40). By contrast, peak isometric active developed tension of mdx cardiac trabeculae was changed relative to the wild type only at the highest frequencies (10 to 12 Hz), whereas the tension of *Cmah*^{-/-}mdx trabeculae was reduced at all frequencies between 4 and 12 Hz ($P < 0.01$ for all versus wild type). The frequencies used here for heart muscle measures are relevant in the mouse; the resting mouse heart beats at ~600 beats per minute (or 10 Hz) and can increase up to 800 beats per minute on stimulation (or ~13 Hz) (111). We also measured Evans blue dye (EBD) uptake, a measure of myofiber membrane damage, into skeletal myofibers after exercise and found that all *Cmah*^{-/-}mdx skeletal muscles had significantly more damage than mdx muscles (Fig. 2E). Similarly, *Cmah*^{-/-}mdx muscles showed increased loss of force during repeated eccentric contractions [in the extensor digitorum longus (EDL) muscle] relative to mdx (Fig. 2F). In none of these instances did *Cmah*-deficient mice with intact dystrophin (*Cmah*^{-/-}) show a significant change relative to wild-type animals (Fig. 2, A to F). Thus, loss of *Cmah* in mice increased the weakness of both cardiac and skeletal muscles only when dystrophin was also deficient, and this effect was particularly clear in diaphragm and heart—the two muscles whose failure typically causes death of DMD patients.

Although mdx mice display histopathology that is reflective of DMD (10, 11), loss of *Cmah* increased many relevant histopathology measures. *Cmah*^{-/-}mdx mice had increased necrotic foci (regions of damage with immune cell infiltrates) by 3 months of age in the heart (Fig. 3A) and increased fibrosis (replacement of skeletal muscle with ECM) by 6 weeks of age in the quadriceps (Fig. 3B). These findings are not present in the larger limb muscles of mdx mice until the mice are very old (10, 11). In addition, the extent of fibrosis in *Cmah*^{-/-}mdx diaphragm, the only mdx muscle where fibrosis is routinely found (40), at 6 months of age was increased relative to mdx mice (Fig. 3C). EBD uptake was also increased, indicating increased myofiber damage in *Cmah*^{-/-}mdx mice (Figs. 2E and 3D). Overall, measures of muscle damage (regions with necrotic myofibers or where muscle tissue was replaced by ECM or inflammatory infiltrates) were significantly increased in the gastrocn-

mius, quadriceps, tibialis anterior, diaphragm, and heart (Fig. 3E). As in DMD (5), the extent of muscle damage varied from muscle to muscle. Other measures of muscle histopathology or damage, including skeletal myofibers with centrally located nuclei (fig. S2A), coefficient of variance in skeletal myofiber diameter (fig. S2B), average myofiber diameter (fig. S2C), and serum creatine kinase activity (fig. S2D), were not significantly different. Mouse (fig. S2E) and muscle (fig. S2F) weights at 5 months of age were decreased in *Cmah*^{-/-}mdx relative to mdx mice. These decreases were independent of changes in average myofiber diameter (fig. S2C) and were therefore also suggestive of increased muscle damage.

Altered protein binding and expression in *Cmah*^{-/-}mdx skeletal muscle

Because sialic acids are abundant in the membranes of all mammalian cells, altering the sialic acid repertoire by eliminating Neu5Gc could alter multiple molecular processes (112). We chose, however, two particular sialic acid-related mechanisms that cause or worsen muscular dystrophy for detailed investigation: the relative strength (and composition) of the DAG complex and the relative immune response to dystrophic muscle tissue. We first investigated the role of the sialyl-containing glycans and their modulation of ECM binding on α DG. Dystroglycan is an essential membrane component of the DAG complex, and binding of muscle ECM proteins, including laminins and agrin, to α DG requires O-mannosyl-linked sialylated tetrasaccharides [Neu5Ac(or Neu5Gc) α 2-3Gal β 1-4GlcNAc β 1-2Man- α -O-Ser/Thr] (24), which are present in the mucin domain of the α DG polypeptide (113). We purified α DG from skeletal muscle of *Cmah*^{-/-} mice, where none of the sialic acid on α DG is Neu5Gc [but instead is all Neu5Ac (109, 110)], and from wild-type skeletal muscle, where Neu5Gc is present (fig. S3, A and B). We also purified recombinant forms of muscle laminins (α 2, α 4, and α 5) and agrin (α 0, muscle; α 8, neural) (fig. S3A). The amount of immobilized α DG was verified to be the same with α DG antibodies that recognize both glycoforms equally well, and the presence or absence of Neu5Gc was confirmed with a Neu5Gc-specific antibody (fig. S3B). Both recombinant laminin α 2 (G1 to G5 domains) (Fig. 4A) and agrin (fig. S4A) bound less well to *Cmah*^{-/-} α DG relative to wild-type α DG (36 \pm 1% decrease for laminin α 2 and 39 \pm 3% for agrin at the highest concentration; $P < 0.001$ for both).

To more directly demonstrate the relevance of Neu5Gc to ECM binding, we also measured binding of sialyl-containing glycans [Neu5Gc(or Neu5Ac) α 2-3Gal β 1-4GlcNAc-biotinylated polyacrylamide (PAA) or Neu5Gc(or Neu5Ac) α 2-6Gal β 1-4GlcNAc-biotinylated PAA] to the same proteins (fig. S4, B and C). Again, we found significant decreases in maximal binding of Neu5Ac-containing glycans to ECM proteins relative to glycans containing Neu5Gc ($P < 0.05$ for all Neu5Gc-PAA versus Neu5Ac-PAA glycans at 500 nM). Similarly, measures of apparent solid-phase binding affinity of α 2-3- and α 2-6-linked Neu5Gc glycans to ECM proteins were increased relative to their Neu5Ac counterparts (fig. S4D). Thus, laminins and agrins have properties consistent with sialic acid-binding lectins, showing a significant binding affinity for sialic acid-containing glycans, particularly α 2-6-linked Neu5Gc glycans, which is independent of the α DG polypeptide. Although the affinity of these glycans for ECM proteins does not match that of the native α DG glycoprotein, the affinity of some glycans was within one log unit of this value (fig. S4D). We concluded that the presence of Neu5Gc on the sarcolemmal membrane strengthens ECM binding, particularly when Neu5Gc glycans are presented in a multivalent form, as here with PAA

conjugation. Such changes are similar to changes in laminin binding to α DG when terminal β 1-4-linked *N*-acetylglucosamine is present (92). Overexpression of Galgt2, the enzyme that produces this carbohydrate, can inhibit mdx muscle damage (38) and pathology (46, 114). Such changes could therefore help to explain the increased damage in *Cmah*^{-/-}mdx muscles.

Other proteins, especially utrophin, α -dystrobrevin, and α - to δ -sarcoglycans, are also important components of the DAG complex in skeletal and cardiac muscle (115). Utrophin, a dystrophin ortholog that is up-regulated in mdx skeletal muscles (116), can ameliorate mdx muscle disease when overexpressed (32) and can increase mdx disease severity when deleted (86, 117), even when only one of the two utrophin alleles is absent (118). Similarly, deletion of α -dystrobrevin, which binds dystrophin and utrophin, in mdx mice amplifies the severity of muscular dystrophy (88). Accordingly, we measured utrophin, α -dystrobrevin, and other DAG member proteins (Fig. 4, E and H to J) and messenger RNA (mRNA) expression (Fig. 4, F and G) in skeletal muscle and heart. Although DAG protein in KCl-washed purified sarcolemmal membranes was originally found to be severely reduced in mdx skeletal muscle (15), such findings were due in part to detergent extraction conditions (25, 26). We (46) and others (25) have found that DAG protein expression is more modestly changed in crude mdx muscle extracts relative to the wild type, and we have used such lysates here (46). mdx skeletal muscles have more utrophin protein than do wild-type muscles, but this compensatory increase was reduced by $30 \pm 2\%$ for utrophin and by $36 \pm 9\%$ for α -dystrobrevin 2 (Fig. 4H). In contrast, we observed no change in *Cmah*^{-/-}mdx muscle (versus mdx) for α - to δ -sarcoglycans, α - and β -dystroglycan, or α -dystrobrevins 3 and 4, although all were reduced in both mdx and *Cmah*^{-/-}mdx muscles relative to wild-type and *Cmah*^{-/-} mice (Fig. 4, E and H), as previously reported (15, 46). Although utrophin and α -dystrobrevin protein were significantly reduced in *Cmah*^{-/-}mdx relative to mdx, mouse IgM and collagens I and III were significantly increased (Fig. 4, E and H). In contrast to skeletal muscle, no decrease in utrophin or α -dystrobrevin protein

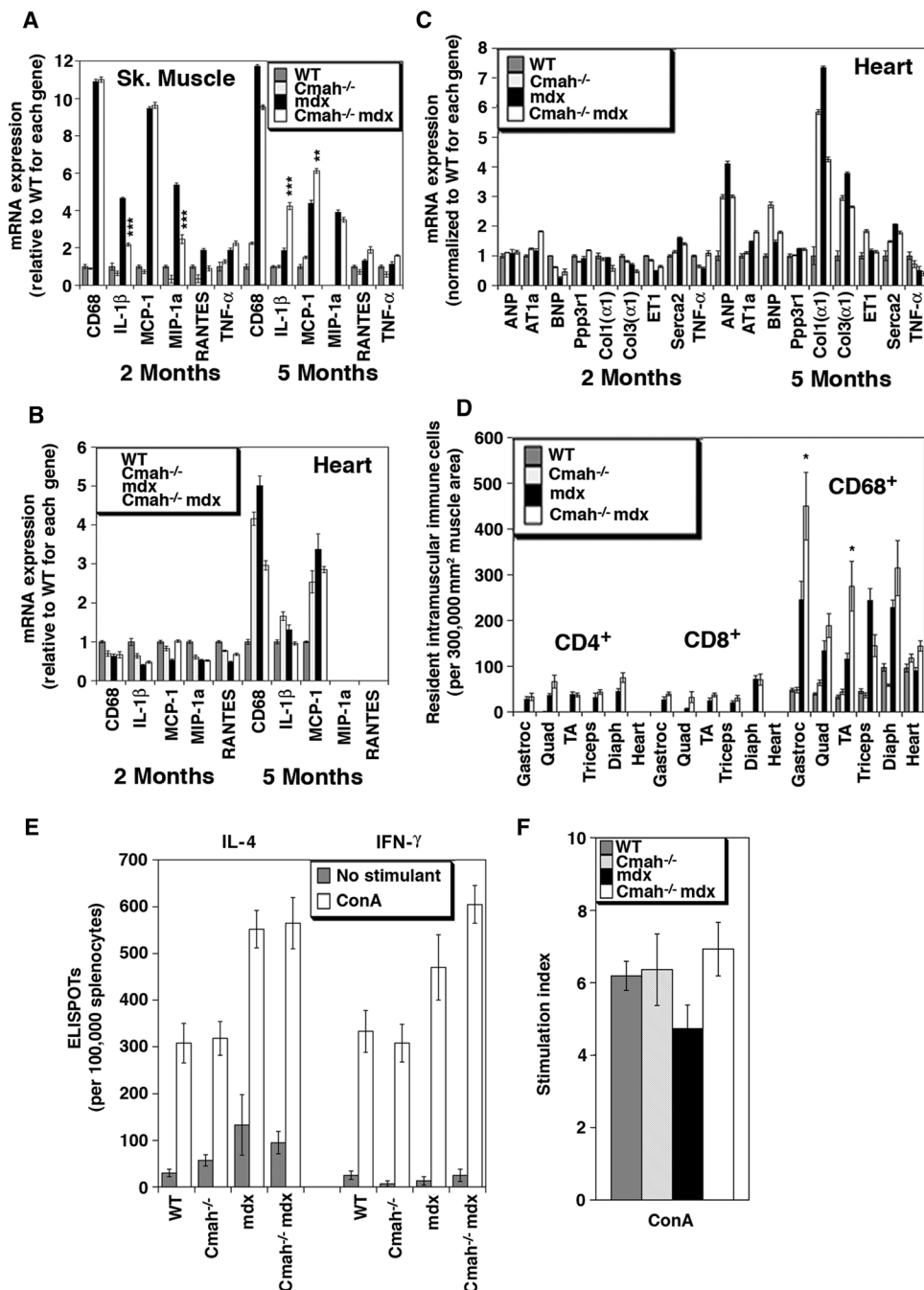


Fig. 5. Measures of immune response in *Cmah*^{-/-}mdx muscle. (A) mRNA expression for markers of muscle inflammation (IL-1 β , MCP-1, and MIP-1a) and macrophage or monocyte infiltration (CD68) was increased in 2- and 5-month-old mdx and *Cmah*^{-/-}mdx skeletal muscles relative to WT. Five-month-old MIP-1a concentrations for WT and *Cmah*^{-/-} were undetectable. (B) mRNA expression of MCP-1 and CD68 was increased in 5-month-old *Cmah*^{-/-}, mdx, and *Cmah*^{-/-}mdx heart ($P < 0.05$ for all versus WT for CD68 and MCP-1). (C) Five-month-old *Cmah*^{-/-}, mdx, and *Cmah*^{-/-}mdx hearts all showed increases in some markers of cardiac hypertrophy. ANP, atrial natriuretic peptide; AT1a, angiotensin II receptor type 1a; BNP, B-type natriuretic peptide; Col1(α 1), collagen type I α 1; Col3(α 1), collagen type III α 1; ET1, endothelin 1. (D) Number of cells per unit muscle area expressing CD4, CD8, or CD68 was quantified in 2-month-old skeletal muscles and heart. Diaph, diaphragm. (E) ELISPOT assays for stimulation of IL-4 or IFN- γ by Con A were compared with splenocytes from WT, *Cmah*^{-/-}, mdx, and *Cmah*^{-/-}mdx mice. No stimulant is buffer alone. (F) Stimulation index was calculated to assess T cell proliferation in response to Con A as compared to no stimulant (buffer alone). Error bars are SEM for $n = 9$ to 12 in (A) to (C) and $n = 6$ in (D) to (F). * $P < 0.05$, ** $P < 0.01$, *** $P < 0.001$.

was observed in *Cmah*^{-/-}mdx heart relative to mdx (Fig. 4, E and I). Here, however, *Cmah*^{-/-} cardiac muscle, in addition to mdx and *Cmah*^{-/-}mdx muscle, showed increased expression of collagens I and III (Fig. 4, I and J), suggesting the presence of fibrosis in *Cmah*^{-/-}, mdx, and *Cmah*^{-/-}mdx heart muscle. The only protein significantly reduced in *Cmah*^{-/-}mdx heart relative to mdx was Serca2 (sarcoplasmic/endoplasmic reticulum calcium transporting adenosine triphosphatase 2) (Fig. 4, I and J), which, along with the increased concentrations of collagens I and III, points to increased cardiac pathology (119). Shorter versions of dystrobrevin were significantly increased in both mdx and *Cmah*^{-/-}mdx heart, whereas dystrobrevin 2, α DG, and α -, β -, and δ -sarcoglycans were decreased in mdx and *Cmah*^{-/-}mdx animals (relative to either wild type or *Cmah*^{-/-}; Fig. 4, E and I; $P < 0.05$ for all).

Consistent with altered concentrations of protein, compensatory increased mRNA expression was observed by quantitative reverse transcription polymerase chain reaction (PCR) for utrophin, α -dystrobrevin, and other DAG and ECM genes in mdx skeletal muscle (Fig. 4F). The extent of increased expression in mdx muscle (versus wild type) was reduced in *Cmah*^{-/-}mdx skeletal muscle for a number of muscle ECM and DAG genes [Fig. 4F; 65 \pm 3% reduction for utrophin, 56 \pm 2% for α -dystrobrevin, 84 \pm 2% for laminin α 2, 56 \pm 2% for laminin α 4, 100 \pm 2% for collagen IV(α 1), 100 \pm 2% for collagen IV(α 2), 56 \pm 2% for agrin, 48 \pm 1% for dystroglycan, and 64 \pm 2% for β -sarcoglycan, $P < 0.01$ for all]. Thus, *Cmah* deletion may globally affect DAG and ECM gene expression in mdx skeletal muscle. Conversely, such changes may reflect the increased dystrophy present in *Cmah*^{-/-}mdx skeletal. mRNA expression for many DAG genes was unchanged in *Cmah*^{-/-}mdx heart (Fig. 4G). The two exceptions here were laminin α 5 and integrin α 7, which were increased in mdx heart (versus wild type) and significantly reduced in *Cmah*^{-/-}mdx heart (Fig. 4G).

To explore molecular changes more broadly, we analyzed transcriptional changes by using Affymetrix microarrays to compare wild-type, *Cmah*^{-/-}, mdx, and *Cmah*^{-/-}mdx skeletal muscle and heart (Fig. 4K). In skeletal muscle, we identified 618 unique gene expression changes (out of 39,000 mouse transcripts analyzed, $P < 0.05$) in *Cmah*^{-/-}mdx relative to mdx, *Cmah*^{-/-}, and wild-type mice and 404 such unique changes in heart. Most genes with changed expression in skeletal muscle (79%) and heart (77%) did not overlap with genes altered in mdx versus wild type or *Cmah*^{-/-} versus wild type. Thus, most gene changes in *Cmah*^{-/-}mdx mice are unique to the combination of dystrophin deficiency and *Cmah* deletion and are not simply an amplification of dystrophic changes found in mdx muscle.

Altered immune responses in *Cmah*^{-/-}mdx mice

Last, we assessed immune responses in mouse muscles (Figs. 5 and 6) because T cell-, macrophage- or monocyte-, and antibody-mediated inflammatory responses all play a role in DMD pathogenesis (11, 120). We first looked at markers of muscle inflammation, focusing on factors that recruit immune cells to skeletal muscles. Gene expression markers of muscle inflammation [CD68; interleukin-1 β (IL-1 β); monocyte chemoattractant protein-1 (MCP-1); macrophage inflammatory protein-1a (MIP-1a); RANTES; and tumor necrosis factor- α (TNF α)] in skeletal muscle were generally higher in both mdx and *Cmah*^{-/-}mdx muscles relative to wild-type and *Cmah*^{-/-} mice, as expected for dystrophic muscles (Fig. 5A). At 2 months, when dystrophy is first present in mdx muscles, we found reduced levels of several markers in *Cmah*^{-/-}mdx mice relative to mdx (IL-1 β and MIP-1a; Fig. 5A), whereas IL-1 β and MCP-1 were increased (by 100 \pm 7% and 35 \pm 3%, respectively) in

Cmah^{-/-}mdx mice relative to mdx at 5 months of age, when dystrophy is more severe (Fig. 5A). Expression of CD68, a macrophage or monocyte marker, was high in both genotypes of mice at both ages. In heart, markers of inflammation were not evident until 5 months of age (Fig. 5B). Here, as with increased collagen protein (Fig. 4, I and J) and gene expression levels (Fig. 5C), we found increased expression of CD68 and MCP-1 in *Cmah*^{-/-} muscle in addition to mdx and *Cmah*^{-/-}mdx, whereas we observed no signal for MIP-1a or RANTES (Fig. 5B). Natriuretic peptide precursor type A levels, which are increased in cardiac hypertrophy, were also increased in all three of these genotypes (Fig. 5C). These data suggest that heart muscle may be subjected to Neu5Gc-dependent phenotypes that are independent of loss of dystrophin. We also quantified (by immunostaining) the numbers of intramuscular-resident macrophages or monocytes (CD68), T helper (T_H) cells (CD4), and cytotoxic T cells (CD8) (Fig. 5D). All three of these cell populations were increased in most mdx and *Cmah*^{-/-}mdx muscles relative to those of wild-type and *Cmah*^{-/-} mice. As expected, most immune cells in mdx and *Cmah*^{-/-}mdx muscles were CD68⁺ macrophages or monocytes—the cells primarily responsible for clearing damaged myofibers (121, 122). Although there was some muscle-to-muscle variability both in resident numbers of intramuscular immune cells and in molecular markers of muscle inflammation, *Cmah*^{-/-}mdx muscles showed no generalized increase in inflammation (relative to mdx muscles) that would explain the increased severity of muscle disease. Several muscles (gastrocnemius, tibialis anterior, and diaphragm, but not quadriceps, triceps, or heart), however, did show increased numbers of CD68⁺ mononuclear cells at 5 months of age (Fig. 5E; $P < 0.05$ for gastrocnemius and tibialis anterior). This increase in intramuscular macrophages and monocytes could reflect increased dystrophy at this age in *Cmah*^{-/-}mdx muscles or increased inflammation that is in turn driving increased dystrophy.

Although overall intramuscular T cell burden was only minimally changed in *Cmah*^{-/-}mdx animals relative to mdx, the T cells present in *Cmah*^{-/-}mdx animals might still be more active than those present in mdx. We tested this in several ways. First, we performed enzyme-linked immunosorbent (ELISPOT) assays of T cell activation using both IL-4 and interferon- γ (IFN- γ) as reporters of T_H2 and T_H1 responses, respectively, as we have done previously (105) (Fig. 5E). Nonstimulated mdx and *Cmah*^{-/-}mdx splenocytes showed a slight elevation in IL-4⁺ ELISPOTs relative to those from wild-type and *Cmah*^{-/-} mice, and both mdx and *Cmah*^{-/-}mdx splenocytes showed higher concanavalin A (Con A) induction of ELISPOTs for IL-4 and IFN- γ compared to wild type and *Cmah*^{-/-} (Fig. 5E). There were no significant differences, however, between *Cmah*^{-/-}mdx and mdx with either measure. We also performed T cell proliferation assays using uptake of [³H]thymidine, as previously (123), to assess whether *Cmah*^{-/-}mdx splenocytes would show a difference in activation of T cell division (Fig. 5F). Con A increased the T cell stimulation index for all four genotypes of mice, but again, there was no difference between mdx and *Cmah*^{-/-}mdx splenocytes. Thus, we found no evidence of a difference in the activation potential of T cells between *Cmah*^{-/-}mdx and mdx mice. We did not assess activation by Neu5Gc directly in these assays because there are no known T cell receptors that can recognize terminal sialic acids on glycans.

Because we had observed incorporation of dietary Neu5Gc specifically in *Cmah*^{-/-}mdx cardiac and skeletal muscle (Fig. 1, B to D), we wanted to determine whether this expression would increase the production of Neu5Gc antibodies because Neu5Gc is a foreign glycan in *Cmah*^{-/-}mdx mice as it is in humans (103). We used α 2-3- or α 2-6-

specific sialic acid lectins to purify skeletal muscle proteins from wild-type muscle, which contains Neu5Gc (fig. S3C), and from *Cmah*^{-/-} muscle, which does not (fig. S3C), to compare serum antibody binding at varying dilutions. Although serum from wild-type, *Cmah*^{-/-}, and mdx mice showed no Neu5Gc-specific titer to either α 2-3- or α 2-6-linked glycoproteins, serum from *Cmah*^{-/-}mdx mice showed Neu5Gc-specific antibody titers as high as 13 μ g/ml (and on average 2 ± 1 μ g/ml) to α 2-6-linked structures (Fig. 6A). This is almost one log unit below the average value identified in studies of human serum, where Neu5Gc-specific antibody titers are also higher to α 2-6-linked sialic acid-containing glycans than to α 2-3-linked ones (103).

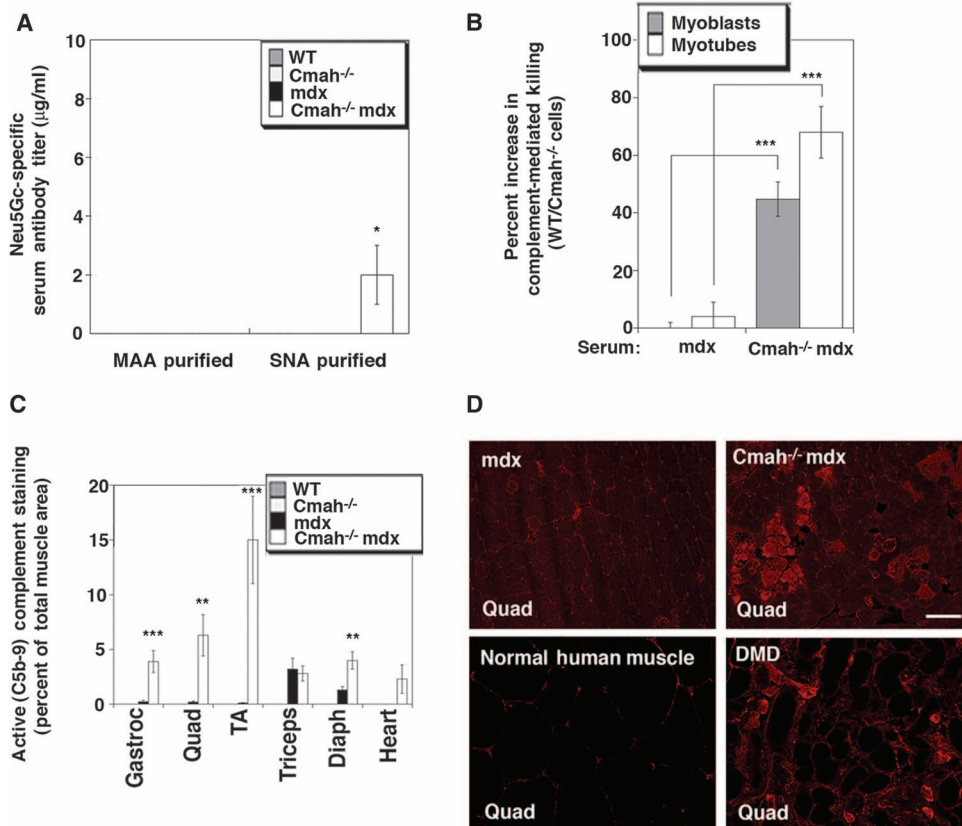
We next determined whether the increased Neu5Gc-dependent antibodies in *Cmah*^{-/-}mdx mouse serum (Fig. 6A) might stimulate complement-mediated killing of Neu5Gc-expressing cells. To do this, we compared the serum of *Cmah*^{-/-}mdx and mdx mice in complement-dependent killing assays (Fig. 6B). Using varying dilutions, we found that serum from *Cmah*^{-/-}mdx mice uniformly increased complement-mediated killing of Neu5Gc-rich cells (wild type) more than Neu5Gc-deficient cells (*Cmah*^{-/-}; Fig. 6B). This was true for cultures of both primary myoblasts and myotubes (Fig. 6B). Serum from mdx mice, by contrast, showed no such difference at any dilution tested (Fig. 6B). This suggests that antibodies to Neu5Gc in *Cmah*^{-/-}mdx serum can drive activation of complement and the killing of Neu5Gc-expressing myoblasts and myotubes. Consistent with this notion, we found that *Cmah*^{-/-}mdx skeletal and cardiac muscles had increased deposition of mouse antibody (Fig. 4E and fig. S6) and activated (C5b-9) complement (Fig. 6, C and D, and figs. S5 and S6). By contrast, there was no deposition of activated (C5b-9) complement or mouse antibody in any wild-type or *Cmah*^{-/-}

muscle (fig. S6). Deposition of activated complement was evident on small regenerating myofibers (or differentiating myoblasts), which were marked by costaining for embryonic myosin, and some such muscles were also positive for Neu5Gc expression (fig. S6). Many myofibers with deposited C5b-9 complement also had deposited endogenous mouse antibody, suggestive of activation of the classical (antibody-mediated) complement pathway (fig. S6). This was not, however, the case in all myofibers (fig. S6). The increased deposition of activated C5b-9 complement, also known as the membrane attack complex, on *Cmah*^{-/-}mdx muscles in vivo would be expected to destroy the myofibers to which it is bound because C5b-9 is the cytotoxic pore-forming complement protein complex (124).

DISCUSSION

The evolution of modern humans from the great apes coincided with a series of genetic changes that altered both the composition of sialic acids on the surface of human cells and the properties of sialic acid-binding proteins (112). Although such changes may have been advantageous for blunting infections by lethal pathogens such as malaria (125), our experiments suggest that deletion of *CMAH* came at the cost of worsening the severity of DMD, caused by genetic inactivation of the dystrophin gene. Although there are certainly additional genetic changes in humans that influence the presentation of DMD disease, the fact that the simple deletion of *Cmah* in mice results in accelerated presentation of dystrophic phenotypes in mdx animals suggests a direct role for sialic acid modifications in muscle disease. Regardless of the exact mechanism by which *Cmah* deletion acts, *Cmah*^{-/-}mdx mice

Fig. 6. Neu5Gc antibody titers and complement deposition and killing in *Cmah*^{-/-}mdx mice. (A) Serum antibody titers to Neu5Gc-containing glycoproteins were compared to titers against Neu5Ac-containing glycoproteins to determine Neu5Gc-specific antibody titers. Skeletal muscle proteins for WT or *Cmah*^{-/-} skeletal muscles were purified with MAA, which purifies α 2-3-linked sialylglycoproteins, or SNA, which purifies α 2-6-linked sialylglycoproteins (see fig. S3C). Only *Cmah*^{-/-}mdx mouse serum showed measurable Neu5Gc-specific titers and only to α 2-6-linked glycoproteins. (B) Serum from *Cmah*^{-/-}mdx and mdx mice was compared for complement-mediated cell killing of Neu5Gc-expressing myoblasts and myotubes from WT mice and Neu5Gc-deficient myoblasts and myotubes from *Cmah*^{-/-} mice. (C) Quantification of the area of muscle deposited with C5b-9 complement. Levels were increased in *Cmah*^{-/-}mdx gastrocnemius, quadriceps, tibialis anterior, diaphragm, and heart relative to mdx. (D) Increased staining of C5b-9 complement in *Cmah*^{-/-}mdx and DMD quadriceps relative to mdx or normal human muscle. Error bars are SEM for *n* = 6 to 12 in (A) to (C). **P* < 0.05, ***P* < 0.01, ****P* < 0.001. Scale bar, 100 μ m (D).



represent a biologically and genetically improved small-animal model for DMD that should facilitate the testing of therapeutics with morbidity and mortality measures more akin to the human disease. Because the current best model for DMD is the dystrophin-deficient golden retriever (GRMD) (98), having a mouse model that can better mimic the more severe aspects of DMD, including increased mortality, increased cardiac and respiratory muscle weakness, and increased deficits in ambulation, should facilitate translational work on these important aspects of DMD. This mouse model will allow drug and gene therapy tests without requiring scale-up of reagent quantities. Because dogs are breeds and not pure genetic strains, the *Cmah*^{-/-}mdx mice will have less genetic variability among animals than GRMD dogs. Dog skeletal muscles also tend to be poor in Neu5Gc content (99), perhaps accounting for the increased severity of disease, as in *Cmah*-null mice.

We have further described two, not mutually exclusive, mechanisms that may contribute to the increased disease severity of *Cmah*^{-/-}mdx animals. The first involves lower levels and function of the DAG complex, including reduced ECM binding to α DG and reduced expression of utrophin, a dystrophin surrogate that when overexpressed can ameliorate disease (61), as well as reduced expression of other DAGs. Although the reduction in DAG protein shown here may seem modest (30 to 35% for utrophin and α 2-dystrobrevin relative to mdx), loss of only one allele of utrophin increases the severity of muscle damage in mdx animals (118). Loss of DAG would contribute to the weakening of sarcolemmal membrane and the integrity of muscle fibers. The second potential mechanism is the metabolic accumulation of dietary Neu5Gc (102), generation of Neu5Gc-specific antibodies (103), and the deposition of activated (C5b-9) complement on muscle fibers. Both activated C5b-9 complement (126) and CD8⁺ cytotoxic T cells (127) are present in DMD muscle, and we have shown here high C5b-9 deposition in young DMD muscle. Because *Cmah*-deficient mdx myofibers, such as DMD myofibers, appear to preferentially take up Neu5Gc from the diet, they may mimic the role in DMD of dietary Neu5Gc in priming immune responses to regenerating muscle, a process that would seed the destruction of the very cells needed to overcome dystrophic muscle damage. This could speed the wasting of skeletal muscle in DMD, the process that ultimately causes muscle failure and mortality in patients. All humans express antibodies that recognize Neu5Gc (103, 104), a foreign antigen in humans, and most humans eat large amounts of Neu5Gc in their diet from Neu5Gc-rich food sources, particularly red meat, which can be incorporated into human cells under certain conditions. The concentrations of Neu5Gc antibodies in *Cmah*^{-/-}mdx mice are lower than those in normal human subjects (103), which implies that our suggested mechanism would be even more important if *Cmah*^{-/-}mdx Neu5Gc antibody concentrations were as high as they are in humans. Because sialic acids are present on many proteins and lipids, and because they are present in all tissues, genetic removal of Neu5Gc in mice likely has effects on many signaling pathways beyond those described here. The broad spectrum of functions influenced by individual cell surface carbohydrates makes the creation of animal disease models that mimic the human glycome all the more imperative.

MATERIALS AND METHODS

Materials

Antibodies to dystrophin (NCL-DYS1), utrophin (NCL-DRP2), α -sarcoglycan (NCL-a-SARC), β -sarcoglycan (NCL-b-SARC), δ -sarcoglycan

(NCL-d-SARC), γ -sarcoglycan (NCL-g-SARC), myosin heavy chain (developmental) (NCL-MHC-d), and β -dystroglycan (NCL-b-DG) were purchased from Novocastra. Antibody to α DG (IIH6C4) was purchased from Upstate Biotechnology. Antibody to α -dystrobrevin (610766) was purchased from BD Transduction Laboratories. Antibodies to actin (A5060) and FLAG [M2; horseradish peroxidase (HRP)- and agarose-conjugated] were purchased from Sigma-Aldrich. Antibody to mouse CD68 (MCA1957Ga) was purchased from Serotec. Antibodies to mouse CD4 (550278) and CD8 (550281) were purchased from BD Pharmingen. Antisera specific for the activated state of complement C5b-9 complex (55811), rabbit polyclonal antibodies to collagen I (ab34710), and collagen III (ab7778) were purchased from Abcam. Mouse monoclonal antibody (MA3-919) to Serca2 was purchased from Thermo Scientific. An additional rabbit polyclonal antiserum specific to Serca2a was a gift from M. Periasamy (Ohio State University). MAA [fluorescein isothiocyanate (FITC)- or agarose-conjugated], *Sambucus nigra* agglutinin (SNA; FITC- or agarose-conjugated), and wheat germ agglutinin (WGA; agarose-conjugated) were purchased from EY Laboratories. Species- and/or antibody-specific secondary antibodies conjugated with FITC, rhodamine, cyanine (Cy2 and Cy3), or HRP were purchased from Jackson Immunochemicals. Methods for production of antibody to Neu5Gc and its specificity for Neu5Gc have been described (109, 110).

Glycans conjugated to PAA (and containing biotin), including Neu5Gc α 2-3Gal β 1-4GlcNAc-PAA, Neu5Ac α 2-3Gal β 1-4GlcNAc-PAA, Neu5Gc α 2-6Gal β 1-4GlcNAc-PAA, Neu5Ac α 2-6Gal β 1-4GlcNAc-PAA, and Gal α 1-3Gal β 1-4GlcNAc-PAA, were obtained from the Consortium for Functional Glycomics (Core D) or purchased from Glycotect. All plasmids used in the production of recombinant proteins have been previously described (92, 128).

Animals

All mice were housed on a 12:12-hour light-dark cycle and had access to a pellet diet (catalog no. 2919, Teklad Global Rodent diet, Harlan) and water ad libitum. The content of Neu5Gc in the diet was measured as 6 μ g of Neu5Gc per gram of mouse chow. This gives a daily consumption dosage, assuming 4 g of mouse chow consumed per day and an average mouse weight of 25 g, of 0.96 mg/kg per day for Neu5Gc. This dosage is perhaps higher than that of a human 30-kg child by a factor of 3, whose dose would be 0.33 mg/kg per day based on an estimated 10 mg Neu5Gc consumed in the diet daily (100). However, absorption of Neu5Gc from the gut into the bloodstream could be considerably different between species and was not studied here. All experimental protocols were reviewed and approved by the Institutional Animal Care and Use Committee of Research Institute at Nationwide Children's Hospital and/or Ohio State University. Wild-type (WT) C57BL/6J and mdx (C57BL/10ScSn-Dmd^{mdx/Y} and C57BL/10ScSn-Dmd^{mdx/mdx}) mice were purchased from the Jackson Laboratory, bred, and maintained in the transgenic barrier facility at the Nationwide Children's Hospital or at Ohio State University. Breeding pairs of *Cmah*-null mice (*Cmah*^{-/-}) were made and described previously (109). These mice carried a human-like deletion of exon 6 of the *Cmah* gene and were generated by embryonic stem cell targeting by the introduction of loxP sites flanking exon 6 and Cre-mediated recombination in embryonic stem cells (109). *Cmah*^{-/-}mdx mice were obtained through creating first and second filial generations by the following strategy. Female mdx/mdx mice were bred with male *Cmah*^{-/-} mice. F1 males (*Cmah*^{+/-}mdx/Y) were then mated with mdx/mdx females to create F2 generations that were all dystrophin-deficient (mdx) and either were heterozygous for deletion

of the *Cmah* locus or contained two WT *Cmah* alleles. *Cmah*^{+/-}mdx/Y and *Cmah*^{+/-}mdx/mdx mice were interbred to obtain *Cmah*^{-/-}mdx mice. *Cmah*^{+/-}mdx and *Cmah*^{+/+}mdx mice generated from the same crosses were used as controls for all experiments and did not differ from one another for any of the measures used. DNA extracted from toe clips was used, as described previously (109), to genotype mice for the *Cmah* deletion by PCR.

Histology and morphometric analysis

Animals were anesthetized and skeletal muscles were rapidly excised and snap-frozen in liquid nitrogen-cooled isopentane. Hearts were rinsed free of blood with ice-cold saline and embedded in optimal cutting temperature embedding medium in a dry ice isopentane slurry. Sections (8 μm) were cut in a cryostat and used for histological and immunohistochemical studies. Histomorphological changes in the muscle were analyzed by routine hematoxylin (72404, Richard Allan Scientific) and eosin (318906, Sigma) staining, as described (107), or with Masson's trichrome stain (HT15-1KT, Sigma). Myofiber diameter and area, central nuclei, and necrotic and fibrotic area were determined with the measurement parameters in the AxioVision LE 4.1 imaging software (Zeiss), as described (107).

For immunostaining or lectin staining, muscles were frozen and sectioned as above. For staining with MAA, SNA, or antibody to activated C5b-9 complement, sections were blocked in 5% bovine serum albumin (BSA) in phosphate-buffered saline (PBS) (pH 7.2). Sections were incubated with FITC-conjugated lectin (10 μg/ml) or with antibody, washed, probed with fluorophore-conjugated secondary antibody if necessary, and then mounted. For Neu5Gc staining (and nonimmune chicken IgY), sections were blocked in PBS with 10% human serum that was confirmed to be Neu5Gc-free. Sections were incubated with Neu5Gc or control antibody (1:500) in blocking solution overnight at 4°C, washed in PBS, and incubated with fluorophore-conjugated goat secondary antibody to chicken IgY (1:250; 703-095-155, Jackson ImmunoResearch). For all other antibodies used, which were antibodies raised in rats, rabbits, mice, or chickens, sections were blocked in PBS containing 10% goat serum, incubated in primary antibody overnight, washed in PBS, and incubated with the appropriate secondary reagent. Quantitation of immune cells per unit area or antibody staining per unit area was done on a Zeiss Axiophot epifluorescence microscope with AxioVision LE 4.1 imaging software. At least 10 sections per muscle were analyzed for each animal to obtain measures, with the entire cross-sectional area considered in each case for regions comprising the muscle in question.

Survivability

Growth and death of C57BL/6J (WT), *Cmah*^{-/-}, *Cmah*^{+/-}mdx, *Cmah*^{+/+}mdx, and *Cmah*^{-/-}mdx mice were recorded daily, and death events were used to plot the survivability curve with GraphPad Prism 4 (version 4.03, GraphPad Software).

Assessment of motor function by rotarod

Rotarod sessions were performed in a room adjacent to the housing room in the vivarium. The mice were first allowed to acclimatize to the new surroundings and train on the rotarod treadmill (Economex Rotarod, Columbus Instruments). To ascertain motor function, we individually placed mice in a neutral position on the immobile rotarod bars. Then, the rotarod was activated at a constant speed of 5 rpm, and the time for each mouse fall off the rod was noted. Motor function was assessed on consecutive days, and the average latency to fall was determined.

Measurements of cardiac and skeletal muscle physiology

Assessment of contractile properties of isolated cardiac trabeculae and papillary muscles was done as described (129). Briefly, small, thin preparations were dissected from the right ventricle, placed in between a force transducer and a stimulator hook in an experimental setup and superfused with Krebs-Henseleit solution at 37°C. Twitch contractions were initiated by delivering 3-ms-wide pulses, and the force response was recorded. This force response was assessed at different lengths, different frequencies, and during infusion of the β-adrenergic agonist isoproterenol. After completion of measurements, muscles were weighed and measures were normalized to muscle weight as before (129).

Assessment of diaphragm muscle strip contractility was done as described (68). Briefly, small linear strips were suspended between a force transducer and a stimulator hook in an experimental setup, and superfused with Krebs-Henseleit solution at 37°C. Tetanic force was assessed by tetani of 600-ms duration, with frequencies ranging from 20 to 250 Hz and pulse width of 1 ms. After measurements, muscles were weighed and cross-sectional area was calculated as previously described (38).

Assessment of EDL contractile parameters was done as described (38). Briefly, isolated EDL muscles were tied to a force transducer and linear servomotor. Twitch contractions at 30°C were elicited and the muscle was stretched to optimal length. Next, one to three tetani, 500 ms in duration with 1-ms pulses at 150 Hz, were imposed on the muscle. This was followed by 10 repeats of eccentric contractions. Per repeat, the muscle was tetanized for 700 ms and stretched by 5% of its initial length during the last 200 ms of the tetanus. After stimulation was halted at $t = 700$ ms, the muscle was taken back to its original length in 200 ms. In between repeats, the muscle remained unstimulated for 2 min. After measurements, muscles were weighed and cross-sectional area was calculated as described (38).

Sarcolemmal membrane integrity by Evans blue dye uptake

Eight hours before treadmill exercise, mice were injected intraperitoneally with EBD (500 μg per 10 g of body weight; E2129, Sigma) dissolved in sterile-filtered PBS. Mice were exercised for a total of 45 min at a speed of 12 m/min for the first 15 min and at 24 m/min for the rest of the period. All animals were killed 36 hours later, and serial sections of skeletal and cardiac muscles were analyzed for EBD uptake by fluorescence microscopy with rhodamine-specific optical filters. EBD uptake in the skeletal muscle was quantified with the measurement parameters in the AxioVision LE 4.1 imaging software, as described (108).

Serum creatine kinase assays

Blood cells were allowed to clot, and serum was separated by centrifugation of clotted cells at 1500g for 10 min. The serum creatine kinase activity was determined in triplicate by an enzyme-coupled absorbance-based kit (CK-SL, Diagnostic Chemicals) following the manufacturer's protocol before storage by freezing at -20°C. The enzyme activity was monitored and calculated by measuring the absorbance at 340 nm every 30 s for 4 min at 25°C, as done previously (107).

Extraction of sialic acid linkage-specific glycoproteins from cardiac or skeletal muscle and enzyme-linked immunosorbent assays

Pooled skeletal muscles and heart tissues from WT or *Cmah*^{-/-} mice were solubilized in tris-buffered saline (TBS) [50 mM tris (pH 7.4), 250 mM NaCl] containing 1% NP-40 and protease inhibitors (78425, Pierce). Total protein was measured by bicinchoninic acid (BCA) protein assay (23227,

Pierce) and used for Western blot analysis or further glycoprotein enrichment. Three different glycan-specific lectins were used for isolating glycoproteins needed for different experimental purposes: WGA, MAA, and SNA. WGA selectively binds to *N*-acetylglucosamine and sialic acid residues, whereas MAA and SNA bind to α 2-3- and α 2-6-linked sialic acids, respectively. For WGA purification, 1.5 mg of total protein extracted from WT and *Cmah*^{-/-} skeletal muscle was enriched for WGA glycoproteins with a glycoprotein isolation kit (89805, Pierce) following the instructions provided. WGA glycoprotein-enriched eluates, rich in dystroglycan, were used for solid-phase binding of laminin and agrin to α DG, with WT muscle protein showing high Neu5Gc expression and *Cmah*^{-/-} muscle showing none, despite having equivalent amounts of α DG (fig. S3B). For MAA or SNA purification, 3 mg of muscle proteins from WT or *Cmah*^{-/-} skeletal muscle or heart was enriched for sialic acid-rich glycoproteins with immobilized MAA and SNA (AK-7801 and A-6802, EY Laboratories). Proteins were incubated overnight with 200 μ l of MAA- and SNA-linked agarose beads at 4°C in a total volume of 2 ml. The beads were washed extensively in TBS with 1% NP-40 at 4°C and eluted in 50 mM Tris (pH 6.8) with 1% SDS containing 0.1% glycerol in a volume of 600 μ l. These samples were used to detect Neu5Gc-specific serum antibodies.

To immobilize MAA- or SNA-purified proteins on enzyme-linked immunosorbent assay (ELISA) plates, we diluted proteins at 1:50 into 50 mM sodium carbonate-bicarbonate (pH 9.6) buffer (to yield 0.02% total SDS) at 4°C overnight onto 96-well ELISA plates in a volume of 100 μ l. Subsequently, plates were washed with TBS and blocked with TBST (TBS with 0.1% Tween 20) for 2 hours at room temperature. Amounts of loaded protein were first measured with a micro-BCA kit (catalog no. 23235, Pierce), and 5 to 10 μ g of protein (an excess of the binding capacity of the well) were loaded per well. The presence of Neu5Gc on glycoproteins in WT muscles, and the absence in *Cmah*^{-/-} muscles, was confirmed with the Neu5Gc-specific IgY antibody (fig. S3C). Wells used to determine Neu5Gc-specific titers were blocked with 10% human serum for 1 hour and then incubated with dilutions (from 1:50 to 1:1600) of mouse serum for 3 hours. After extensive washing in TBST, plates were incubated in TBST containing HRP-conjugated goat secondary antibody to mouse for 1 hour and then washed again in TBST. Signal was developed with SIGMAFAST OPD (*o*-phenylenediamine dihydrochloride) (P9187, Sigma), and absorbance was read at 30 min at 450 nm on a plate reader (SpectraMax M2, Molecular Devices). Binding of Neu5Gc-specific mouse antibodies from the serum WT, *Cmah*^{-/-}, mdx, and *Cmah*^{-/-}mdx mice was determined by measuring the positive Neu5Gc-specific signal [WT-(*Cmah*^{-/-}), both corrected for background] and comparing this to goat secondary antibody to mouse IgG and IgM immobilized at different concentrations on the same plate and developed with secondary reagent. Binding of mouse serum antibodies to wells not coated with protein was uniformly minimal (<10% of signal), as was binding of secondary reagents to wells containing immobilized laminin or agrin proteins. Only signals comparing quantities in the linear range (absorbance, 0.1 to 1) were used for measurements of antibody levels.

Growth and transfection of cultured cell lines

Human embryonic kidney-293T (HEK293T) cells were grown in Dulbecco's modified Eagle's medium (DMEM) containing 10% fetal calf serum (FCS), streptomycin (50 μ g/ml), and penicillin (50 U/ml). Cells were transfected with Effectene Reagent (Qiagen) according to the manufacturer's instructions to produce recombinant laminin or agrin proteins.

Expression and purification of recombinant laminins and agrins

Partial complementary DNAs (cDNAs) encoding recombinant, secreted, and FLAG-tagged muscle agrin (G2 and G3, z0), neural agrin (G2 and G3, z8), and the G1 to G5 domains of laminin α 2, laminin α 4, or laminin α 5 were done as previously described (92). Briefly, plasmids were transfected into HEK293T cells with Effectene (301425, Qiagen), and culture supernatants or cell lysates were collected after 48 hours, as previously described (92, 128). After the addition of protease inhibitors, the culture supernatant or lysate was subjected to affinity purification on M2 agarose, and FLAG-labeled proteins were eluted with 3 \times FLAG peptide (F4799, Sigma). 3 \times FLAG peptide was eliminated by extensive washing with a 10,000-dalton molecular mass filter. The expression of recombinant, epitope-tagged proteins was verified by Western analysis with HRP-conjugated monoclonal antibody to FLAG (M2; A8592, Sigma), and purity was assessed by silver stain (24597, Pierce) of eluates after separation by SDS-polyacrylamide gel electrophoresis (SDS-PAGE), all as before (92).

Western blot analysis

Total muscle cell protein (40 μ g) was separated on 10, 12, or 4 to 15% gradient gels by SDS-PAGE and transferred to nitrocellulose membrane. For the detection of α DG, the membranes were blocked and washed in low-salt (100 mM) TBS (pH 7.4). Neu5Gc antibody blots were blocked in TBS containing 0.1% Tween 20 and 20% human serum, and all washes were performed in TBS containing 0.1% Tween 20. For all the other immunoblots, the membranes were blocked with TBS containing 5% nonfat dry milk, 1% BSA, and 0.05% Tween 20. Western blot protein band intensities were quantified as previously described (46, 130). Densitometric scanning of Western blots to quantify relative changes in protein expression between genotypes, relative to WT, was done as previously described (130, 131).

Solid-phase binding assay of ECM proteins to α DG

Solid-phase assays were carried out following a published method (24). WGA glycoproteins were diluted 1:25 in carbonate-bicarbonate buffer (pH 9.6) and coated overnight on polystyrene ELISA microplates (9018, Costar) at 4°C. Plates were washed six times in binding buffer [20 mM Tris (pH 7.4), 150 mM NaCl, 1 mM CaCl₂, and 1 mM MgCl₂] and blocked for 2 hours in binding buffer containing 3% BSA. Purified recombinant laminin α 2 (G1 to G5 domains) and muscle agrin (G2 and G3, z0) were diluted in binding buffer containing 3% BSA and incubated for 2.5 hours. Wells were washed six times with 3% BSA in binding buffer, exposed to peroxidase-conjugated monoclonal antibody to FLAG (M2; 1:500; A8592, Sigma) for 1 hour, washed, and developed with SIGMAFAST OPD. The absorbance was detected at 450 nm (SpectraMax M2).

Solid-phase binding of synthetic carbohydrates to ECM proteins

PAA-linked glycans also containing biotin were obtained from the Consortium for Functional Glycomics (Core D) (Scripps Research Institute) or purchased from Glycotect. All glycans were purified to ~95% purity as analyzed by thin-layer chromatography and ¹H nuclear magnetic resonance and/or mass spectrometry. PAA glycans used were 30 kD and contained 20% glycan and 5% biotin. As such, the valency of glycan to PAA was ~6:1 for each glycan used. All glycans were first verified to have equivalent concentrations of biotin by immo-

bilizing them on ELISA plates, as before (132), and by probing with streptavidin-HRP.

To study PAA glycan binding to recombinant laminins or agrins, we immobilized a monoclonal antibody to FLAG (M2) on ELISA plates at a concentration of 500 ng per well in carbonate-bicarbonate buffer (50 mM, pH 9.5) overnight at 4°C. Wells were blocked with ELISA buffer for 1 hour. Purified agrins [C45 (z0) or C45 (z8)] or laminins (G1 to G5; $\alpha 2$, $\alpha 4$, or $\alpha 5$) were added to each well at 200 ng per well and incubated overnight at 4°C. PAA glycan binding to all five proteins was done in each experiment. After washing, representative wells were incubated in SDS denaturing buffer, separated by SDS-PAGE, and immunoblotted with M2 antibody to verify whether equivalent amounts of protein were present and analyzed by silver staining (24597, Pierce) to determine their relative purity. PAA glycans were added in 100 μ l of binding buffer at concentrations ranging from 0.25 to 3 μ g per well for 2 hours (yielding an effective concentration range of 42 to 500 nM), followed after washing and incubation with peroxidase-conjugated streptavidin (1:1000, for 1 hour). After subsequent washes, plates were developed in SIGMAFAST OPD.

All binding was followed at 5-min intervals for 30 to 60 min, and only data representative of the linear range of response were used for analysis. Absorbance signals varied between 0.1 and 1.0. All data points used represent triplicate measures of each condition. Binding of PAA glycans to wells coated with M2 antibody but not with ECM protein was negligible (<10% of signal), as was binding of secondary reagents to wells containing immobilized laminin or agrin proteins. Aliquots of PAA glycans added for the 3 μ g per well concentration were immobilized on ELISA plates and probed with streptavidin-HRP to verify whether equivalent concentrations of biotin were present (fig. S3D). Estimates of solid-phase binding affinity (fig. S4D) were done by plotting binding curve with a standard receptor binding model (fractional ligand binding = $[L]/(K_d + [L])$ with XLfit software (ID Business Solutions).

Extraction and purification of total skeletal or cardiac muscle mRNA

Gastrocnemius and cardiac muscles dissected out under ribonuclease-free conditions were stored overnight at 4°C in RNAlater (Ambion). The RNAlater was decanted, and tissues were kept frozen at -80°C until RNA extraction. Total RNA was isolated with Trizol reagent (Invitrogen) and further purified on a silica gel-based membrane (RNeasy Mini, Qiagen). Disposable RNA chips (Agilent RNA 6000 Nano LabChip kit) were used to determine the purity or integrity of RNA samples with Agilent Bioanalyzer 2100. RNA content and quality was assessed with an ND-1000 spectrophotometer (NanoDrop). Only samples with a 260/280 absorbance ratio of 2.0 to 2.1 were used for subsequent analysis.

cDNA synthesis and TaqMan gene expression assays

High-Capacity cDNA Archive kit (Applied Biosystems) was used to reverse-transcribe 3 μ g of total RNA following the instructions provided. Samples were subjected to real-time PCR in triplicate on a TaqMan ABI 7500 Sequence Detection System (Applied Biosystems) with 18S ribosomal RNA (4308329, Applied Biosystems) as internal control. Primers and probes were purchased as predeveloped 20 \times TaqMan assay reagents from Applied Biosystems, and the details are provided in table S7. 18S ribosomal RNA probe contained VIC dye as the reporter, whereas the other probes had FAM reporter dye at the 5' end. Each 25- μ l PCR reaction mix consisted of 1 \times primer-probe mix, 1 \times TaqMan Universal

PCR master mix with AmpliTaq Gold DNA polymerase, uracil-*N*-glycosylase (AmpErase), deoxynucleotide triphosphates with deoxyuridine triphosphate, and a passive reference to minimize background fluorescence fluctuations (4304437, Applied Biosystems). After an initial hold of 2 min at 50°C to allow activation of AmpErase and 10 min at 95°C to activate the AmpliTaq polymerase, the samples were cycled 40 times at 95°C for 15 s and at 60°C for 1 min. Gene expression was determined as relative changes by the $2^{-\Delta\Delta C_t}$ method compared to 18S RNA (133), and the data were presented as fold difference relative to WT.

Affymetrix GeneChip expression profiling and analysis

The Ovation Biotin RNA Amplification and Labeling System (NuGen Technologies) was used to prepare amplified biotin-labeled cDNA from total RNA following the manufacturer's instructions. Briefly, first-strand cDNA was synthesized from 25 ng of total RNA with a unique first-strand DNA or RNA chimeric primer and reverse transcriptase. After double-strand cDNA generation, amplification of cDNA was achieved with an isothermal DNA amplification process that involves repeated SPIA DNA or RNA primer binding, DNA duplication, strand displacement, and RNA cleavage. The amplified SPIA cDNA was purified and subjected to a two-step fragmentation and labeling process. The fragmented or biotinylated cDNA content was measured in an ND-1000 spectrophotometer, and the quality was analyzed on an RNA 6000 Nano LabChip (Agilent) with Agilent Bioanalyzer 2100.

For each microarray, cDNA was hybridized onto 430 2.0 GeneChips (Affymetrix), containing probe sets that measure 39,000 transcripts from mouse RNA. The probes were designed on the basis of the gene sequences available in GenBank, dbEST, and RefSeq. The sequence clusters were created from the UniGene database and then refined by analysis and comparison with the publicly available draft assembly of the mouse genome from the Whitehead Institute for Genome Research. Hybridization was allowed to continue for 16 hours at 45°C followed by washing and staining of microarrays in a Fluidics Station 450 (Affymetrix). GeneChips were scanned in a GeneChip Scanner 3000 (Affymetrix), and CEL files were generated from DAT files with GeneChip Operating Software (GCOS) software (Affymetrix). The probe set signals were generated with the robust multichip average (RMA) algorithm in ArrayAssist 3.4 (Stratagene) and used to determine differential gene expression by pair-wise comparisons. The genes that were altered by a factor of 2 either way were sorted and used for further interpretation of the microarray data.

Hierarchical clustering and Venn diagram

The clustering analysis was performed, and Venn diagrams were created by GeneMaths Software 2.01 (Applied Maths). Array-based dendrograms were generated by subjecting the differentially expressed genes to an unsupervised two-dimensional hierarchical clustering algorithm, with Pearson correlation as similarity coefficient and UPGMA (unweighted pair-group method using arithmetic averages) as clustering method. Independent Welch *t* tests followed by Bonferroni procedure were carried out to estimate the number of gene expression changes in *Cmah*^{-/-}, *mdx*, and *Cmah*^{-/-}*mdx* relative to WT, and Venn diagrams were generated to determine the number of unique and common gene expression changes within each group.

ELISPOT assays

Spleens were dissected from WT, *Cmah*^{-/-}, *mdx*, and *Cmah*^{-/-}*mdx* mice, and splenocytes were made by trituration in RPMI 1640 and

filtration through a cell strainer. Cells were then collected by gentle centrifugation (1000g for 3 min). After further purification, splenocytes were cultured at 4×10^5 cells per well and stimulated with Con A (10 $\mu\text{g/ml}$) (a positive control) or buffer alone (a negative control) in the presence of tissue culture media (RPMI 1640 with 10% FCS and penicillin-streptomycin) for 48 hours. Plates were washed in PBS six times and subjected to ELISPOT assays for IL-4, to detect T_{H2} -type responses (CT319-PB5, U-CyTech), or IFN- γ , to detect T_{H1} -type responses (CT317-PB5, U-CyTech), according to the manufacturer's instructions. Spots per well were counted manually after imaging of plates on a Zeiss bright-field microscope with Zeiss imaging software.

T cell proliferation assays

Analysis of T cell proliferation was performed with splenocyte cultures from individual animals. Splenocytes were isolated from WT, *Cmah*^{-/-}, mdx, and *Cmah*^{-/-}mdx animals. At the time of killing, the spleen was dissected and splenocytes were isolated as above (ELISPOT assays). For proliferation assays, 6×10^5 isolated splenocytes were cultured per well (in 96-well ELISA plates) and incubated with control buffer or Con A (10 $\mu\text{g/ml}$) for 48 hours in RPMI medium. After 48 hours of stimulation, 2 μCi of [³H]thymidine (TRK 424, GE Healthcare) was added for an additional 24 hours. Cells were subsequently washed and lysed with a Wallac harvester, and ³H was measured with a scintillation counter. Stimulation index was determined as described (134).

Isolation and growth of primary myoblasts and myotubes

Primary myoblasts were isolated following a published protocol (135). Briefly, leg skeletal muscles were dissected after euthanasia under sterile conditions and minced into tiny bits in PBS containing trypsin (1.5 mg/ml; Mediatech), collagenase D (1.0 mg/ml; Roche), and deoxyribonuclease I (2 mg/ml; Boehringer Mannheim) for 20 min. Tissue digest was triturated, and trypsin was inactivated with DMEM containing 20% FCS, 4% chick embryo extract (US Biologicals), and antibiotics (penicillin-streptomycin). Cells were centrifuged, re triturated in growth medium, and preplated on tissue culture plastic for 20 min at 37°C to remove fibroblasts, and the supernatant was plated on cell culture dishes coated with calf skin collagen (Sigma-Aldrich). Nearly confluent myoblasts were differentiated into myotubes by replacing the medium with DMEM containing 2% horse serum and antibiotics (penicillin-streptomycin), with repeated feeding, for 6 days.

Complement-mediated cell killing assays

Myoblasts were seeded in 96-well tissue culture plates at a density of 5×10^4 cells per well. After 12 to 18 hours, the growth medium was replaced with 50 μl of DMEM without phenol red (Mediatech). Test serum was diluted 1:100 in DMEM without phenol red and added to the cells in a volume of 50 μl . After a 15-min incubation at 37°C, the cells were washed in DMEM without phenol red and exposed to 5% Low-Tox-H rabbit complement (Cedarlane Labs) in DMEM without phenol red. The cells were incubated at 37°C for 1 hour and centrifuged. The supernatant (50 μl) was mixed with 50 μl of lactic acid dehydrogenase (LDH) substrate, and LDH activity was measured following the manufacturer's instruction (Roche Applied Science). The percentage of lysis was calculated with the formula $100 \times [(A - C)/(B - C)]$, where A represents an absorbance obtained with test serum (experimental release), B represents an absorbance obtained by lysing all of the target cells with 1% Triton X-100 (maximum release), and C represents an absorbance obtained with target cells incubated in serum-free medium containing

rabbit complement at 5% (minimum release). Experimental release typically ranged from 10 to 30% of maximal release after correction for background. To measure complement-mediated killing in myotubes, we differentiated the myoblasts into myotubes before conducting the complement-dependent cytotoxicity assay.

Statistics

Either ANOVA (analysis of variance) with repeated measures, where applicable (three or more groups), followed by a post hoc *t* test, or paired or unpaired two-tailed Student's *t* test, where applicable (only two groups), was used to test for statistical differences. Values of $P < 0.05$ (two-tailed) were considered significant.

SUPPLEMENTARY MATERIAL

www.sciencetranslationalmedicine.org/cgi/content/full/2/42/42ra54/DC1

Fig. S1. Characterization of Neu5Gc and sialic acid expression in dystrophic and normal mice and humans.

Fig. S2. Analysis of histopathology and muscle features in *Cmah*-deficient mdx animals.

Fig. S3. Characterization of materials used for binding assays and serum titers.

Fig. S4. Binding of recombinant agrins and laminins to αDG glycoforms and to Neu5Gc and Neu5Ac sialylglycoconjugates.

Fig. S5. Staining of heart and skeletal muscles with antibody to activated C5b-9 complement.

Fig. S6. Coexpression of activated (C5b-9) complement with embryonic myosin, Neu5Gc, and endogenous mouse antibody in *Cmah*^{-/-}mdx muscle.

Table S1. TaqMan gene expression assays used for real-time PCR.

REFERENCES AND NOTES

1. E. P. Hoffman, R. H. Brown Jr., L. M. Kunkel, Dystrophin: The protein product of the Duchenne muscular dystrophy locus. *Cell* **51**, 919–928 (1987).
2. M. Koenig, E. P. Hoffman, C. J. Bertelson, A. P. Monaco, C. Feener, L. M. Kunkel, Complete cloning of the Duchenne muscular dystrophy (DMD) cDNA and preliminary genomic organization of the DMD gene in normal and affected individuals. *Cell* **50**, 509–517 (1987).
3. A. E. Emery, Population frequencies of inherited neuromuscular diseases—a world survey. *Neuromuscul. Disord.* **1**, 19–29 (1991).
4. A. Y. Manzur, F. Muntoni, Diagnosis and new treatments in muscular dystrophies. *Postgrad. Med. J.* **85**, 622–630 (2009).
5. M. H. Brooke, G. M. Fenichel, R. C. Griggs, J. R. Mendell, R. Moxley, J. P. Miller, M. A. Province, Clinical investigation in Duchenne dystrophy: 2. Determination of the “power” of therapeutic trials based on the natural history. *Muscle Nerve* **6**, 91–103 (1983).
6. J. R. Mendell, R. T. Moxley, R. C. Griggs, M. H. Brooke, G. M. Fenichel, J. P. Miller, W. King, L. Signore, S. Pandya, J. Florence, J. Schierbecker, J. Robison, K. Kaiser, S. Mandel, C. Arfken, B. Gilder, Randomized, double-blind six-month trial of prednisone in Duchenne's muscular dystrophy. *N. Engl. J. Med.* **320**, 1592–1597 (1989).
7. G. M. Fenichel, J. M. Florence, A. Pestronk, J. R. Mendell, R. T. Moxley III, R. C. Griggs, M. H. Brooke, J. P. Miller, J. Robison, W. King, L. Signore, S. Pandya, J. Schierbecker, B. Wilson, Long-term benefit from prednisone therapy in Duchenne muscular dystrophy. *Neurology* **41**, 1874–1877 (1991).
8. G. Bulfield, W. G. Siller, P. A. Wight, K. J. Moore, X chromosome-linked muscular dystrophy (*mdx*) in the mouse. *Proc. Natl. Acad. Sci. U.S.A.* **81**, 1189–1192 (1984).
9. P. Sicinski, Y. Geng, A. S. Ryder-Cook, E. A. Barnard, M. G. Darlison, P. J. Barnard, The molecular basis of muscular dystrophy in the mdx mouse: A point mutation. *Science* **244**, 1578–1580 (1989).
10. G. B. Banks, J. S. Chamberlain, The value of mammalian models for Duchenne muscular dystrophy in developing therapeutic strategies. *Curr. Top. Dev. Biol.* **84**, 431–453 (2008).
11. R. Willmann, S. Possekel, J. Dubach-Powell, T. Meier, M. A. Ruegg, Mammalian animal models for Duchenne muscular dystrophy. *Neuromuscul. Disord.* **19**, 241–249 (2009).
12. J. M. Ervasti, K. Ohlendieck, S. D. Kahl, M. G. Gaver, K. P. Campbell, Deficiency of a glycoprotein component of the dystrophin complex in dystrophic muscle. *Nature* **345**, 315–319 (1990).
13. J. M. Ervasti, K. P. Campbell, Membrane organization of the dystrophin-glycoprotein complex. *Cell* **66**, 1121–1131 (1991).

14. O. Ibraghimov-Beskrovnaya, J. M. Ervasti, C. J. Leveille, C. A. Slaughter, S. W. Sernett, K. P. Campbell, Primary structure of dystrophin-associated glycoproteins linking dystrophin to the extracellular matrix. *Nature* **355**, 696–702 (1992).
15. K. Matsumura, J. M. Ervasti, K. Ohlendieck, S. D. Kahl, K. P. Campbell, Association of dystrophin-related protein with dystrophin-associated proteins in *mdx* mouse muscle. *Nature* **360**, 588–591 (1992).
16. J. M. Ervasti, K. P. Campbell, A role for the dystrophin-glycoprotein complex as a transmembrane linker between laminin and actin. *J. Cell Biol.* **122**, 809–823 (1993).
17. J. R. Mendell, D. R. Boué, P. T. Martin, The congenital muscular dystrophies: Recent advances and molecular insights. *Pediatr. Dev. Pathol.* **9**, 427–443 (2006).
18. P. T. Martin, Mechanisms of disease: Congenital muscular dystrophies—glycosylation takes center stage. *Nat. Clin. Pract. Neurol.* **2**, 222–230 (2006).
19. P. T. Martin, The dystroglycanopathies: The new disorders of O-linked glycosylation. *Semin. Pediatr. Neurol.* **12**, 152–158 (2005).
20. C. Jimenez-Mallebrera, S. C. Brown, C. A. Sewry, F. Muntoni, Congenital muscular dystrophy: Molecular and cellular aspects. *Cell. Mol. Life Sci.* **62**, 809–823 (2005).
21. A. Y. Chiu, J. R. Sanes, Development of basal lamina in synaptic and extrasynaptic portions of embryonic rat muscle. *Dev. Biol.* **103**, 456–467 (1984).
22. P. T. Martin, Dystroglycan glycosylation and its role in matrix binding in skeletal muscle. *Glycobiology* **13**, 55R–66R (2003).
23. P. T. Martin, Glycobiology of the neuromuscular junction. *J. Neurocytol.* **32**, 915–929 (2003).
24. D. E. Michele, R. Barresi, M. Kanagawa, F. Saito, R. D. Cohn, J. S. Satz, J. Dollar, I. Nishino, R. I. Kelley, H. Somer, V. Straub, K. D. Mathews, S. A. Moore, K. P. Campbell, Post-translational disruption of dystroglycan–ligand interactions in congenital muscular dystrophies. *Nature* **418**, 417–422 (2002).
25. S. Daval, C. Rocher, Y. Chérel, E. Le Rumeur, Several dystrophin-glycoprotein complex members are present in crude surface membranes but they are sodium dodecyl sulphate invisible in KCl-washed microsomes from *mdx* mouse muscle. *Cell. Mol. Biol. Lett.* **15**, 134–152 (2010).
26. N. Cluchague, C. Moreau, C. Rocher, S. Pottier, G. Leray, Y. Chérel, E. Le Rumeur, β -Dystroglycan can be revealed in microsomes from *mdx* mouse muscle by detergent treatment. *FEBS Lett.* **572**, 216–220 (2004).
27. D. R. Love, D. F. Hill, G. Dickson, N. K. Spurr, B. C. Byth, R. F. Marsden, F. S. Walsh, Y. H. Edwards, K. E. Davies, An autosomal transcript in skeletal muscle with homology to dystrophin. *Nature* **339**, 55–58 (1989).
28. I. N. Rybakova, J. L. Humston, K. J. Sonnemann, J. M. Ervasti, Dystrophin and utrophin bind actin through distinct modes of contact. *J. Biol. Chem.* **281**, 9996–10001 (2006).
29. I. N. Rybakova, J. R. Patel, K. E. Davies, P. D. Yurchenko, J. M. Ervasti, Utrophin binds laterally along actin filaments and can couple costameric actin with sarcolemma when overexpressed in dystrophin-deficient muscle. *Mol. Biol. Cell* **13**, 1512–1521 (2002).
30. W. Chung, J. T. Campanelli, WW and EF hand domains of dystrophin-family proteins mediate dystroglycan binding. *Mol. Cell Biol. Res. Commun.* **2**, 162–171 (1999).
31. J. A. Rafael, J. M. Tinsley, A. C. Potter, A. E. Deconinck, K. E. Davies, Skeletal muscle-specific expression of a utrophin transgene rescues utrophin-dystrophin deficient mice. *Nat. Genet.* **19**, 79–82 (1998).
32. J. Tinsley, N. Deconinck, R. Fisher, D. Kahn, S. Phelps, J. M. Gillis, K. Davies, Expression of full-length utrophin prevents muscular dystrophy in *mdx* mice. *Nat. Med.* **4**, 1441–1444 (1998).
33. A. M. Connolly, R. M. Keeling, S. Mehta, A. Pestronk, J. R. Sanes, Three mouse models of muscular dystrophy: The natural history of strength and fatigue in dystrophin-, dystrophin/utrophin-, and laminin $\alpha 2$ -deficient mice. *Neuromuscul. Disord.* **11**, 703–712 (2001).
34. Y. Tanabe, K. Esaki, T. Nomura, Skeletal muscle pathology in X chromosome-linked muscular dystrophy (*mdx*) mouse. *Acta Neuropathol.* **69**, 91–95 (1986).
35. C. Dellorusso, R. W. Crawford, J. S. Chamberlain, S. V. Brooks, Tibialis anterior muscles in *mdx* mice are highly susceptible to contraction-induced injury. *J. Muscle Res. Cell Motil.* **22**, 467–475 (2001).
36. P. Moens, P. H. Baatsen, G. Maréchal, Increased susceptibility of EDL muscles from *mdx* mice to damage induced by contractions with stretch. *J. Muscle Res. Cell Motil.* **14**, 446–451 (1993).
37. B. J. Petrof, J. B. Shrager, H. H. Stedman, A. M. Kelly, H. L. Sweeney, Dystrophin protects the sarcolemma from stresses developed during muscle contraction. *Proc. Natl. Acad. Sci. U.S.A.* **90**, 3710–3714 (1993).
38. P. T. Martin, R. Xu, L. R. Rodino-Klapac, E. Oglesbay, M. Camboni, C. L. Montgomery, K. Shontz, L. G. Chicoine, K. R. Clark, Z. Sahenk, J. R. Mendell, P. M. Janssen, Overexpression of *Galgt2* in skeletal muscle prevents injury resulting from eccentric contractions in both *mdx* and wild-type mice. *Am. J. Physiol. Cell Physiol.* **296**, C476–C488 (2009).
39. S. V. Brooks, J. A. Faulkner, Contractile properties of skeletal muscles from young, adult and aged mice. *J. Physiol.* **404**, 71–82 (1988).
40. H. H. Stedman, H. L. Sweeney, J. B. Shrager, H. C. Maguire, R. A. Panettieri, B. Petrof, M. Narusawa, J. M. Leferovich, J. T. Sladky, A. M. Kelly, The *mdx* mouse diaphragm reproduces the degenerative changes of Duchenne muscular dystrophy. *Nature* **352**, 536–539 (1991).
41. J. A. Faulkner, R. Ng, C. S. Davis, S. Li, J. S. Chamberlain, Diaphragm muscle strip preparation for evaluation of gene therapies in *mdx* mice. *Clin. Exp. Pharmacol. Physiol.* **35**, 725–729 (2008).
42. P. R. Turner, T. Westwood, C. M. Regen, R. A. Steinhardt, Increased protein degradation results from elevated free calcium levels found in muscle from *mdx* mice. *Nature* **335**, 735–738 (1988).
43. P. Y. Fong, P. R. Turner, W. F. Denetclaw, R. A. Steinhardt, Increased activity of calcium leak channels in myotubes of Duchenne human and *mdx* mouse origin. *Science* **250**, 673–676 (1990).
44. R. Matsuda, A. Nishikawa, H. Tanaka, Visualization of dystrophic muscle fibers in *mdx* mouse by vital staining with Evans blue: Evidence of apoptosis in dystrophin-deficient muscle. *J. Biochem.* **118**, 959–964 (1995).
45. E. Ozawa, Y. Hagiwara, M. Yoshida, Creatine kinase, cell membrane and Duchenne muscular dystrophy. *Mol. Cell. Biochem.* **190**, 143–151 (1999).
46. H. H. Nguyen, V. Jayasinha, B. Xia, K. Hoyte, P. T. Martin, Overexpression of the cytotoxic T cell GalNAc transferase in skeletal muscle inhibits muscular dystrophy in *mdx* mice. *Proc. Natl. Acad. Sci. U.S.A.* **99**, 5616–5621 (2002).
47. G. T. Carter, M. A. Wineinger, S. A. Walsh, S. J. Horasek, R. T. Abresch, W. M. Fowler Jr., Effect of voluntary wheel-running exercise on muscles of the *mdx* mouse. *Neuromuscul. Disord.* **5**, 323–332 (1995).
48. T. Okano, K. Yoshida, A. Nakamura, F. Sasazawa, T. Oide, S. Takeda, S. Ikeda, Chronic exercise accelerates the degeneration-regeneration cycle and downregulates insulin-like growth factor-1 in muscle of *mdx* mice. *Muscle Nerve* **32**, 191–199 (2005).
49. D. Townsend, S. Yasuda, S. Li, J. S. Chamberlain, J. M. Metzger, Emergent dilated cardiomyopathy caused by targeted repair of dystrophic skeletal muscle. *Mol. Ther.* **16**, 832–835 (2008).
50. S. De la Porte, S. Morin, J. Koenig, Characteristics of skeletal muscle in *mdx* mutant mice. *Int. Rev. Cytol.* **191**, 99–148 (1999).
51. J. P. Lefaucheur, C. Pastoret, A. Sebillé, Phenotype of dystrophinopathy in old *mdx* mice. *Anat. Rec.* **242**, 70–76 (1995).
52. J. G. Quinlan, H. S. Hahn, B. L. Wong, J. N. Lorenz, A. S. Wenisch, L. S. Levin, Evolution of the *mdx* mouse cardiomyopathy: Physiological and morphological findings. *Neuromuscul. Disord.* **14**, 491–496 (2004).
53. L. R. Bridges, The association of cardiac muscle necrosis and inflammation with the degenerative and persistent myopathy of MDX mice. *J. Neurol. Sci.* **72**, 147–157 (1986).
54. J. S. Chamberlain, J. Metzger, M. Reyes, D. Townsend, J. A. Faulkner, Dystrophin-deficient *mdx* mice display a reduced life span and are susceptible to spontaneous rhabdomyosarcoma. *FASEB J.* **21**, 2195–2204 (2007).
55. P. Gregorevic, M. J. Blankinship, J. M. Allen, R. W. Crawford, L. Meuse, D. G. Miller, D. W. Russell, J. S. Chamberlain, Systemic delivery of genes to striated muscles using adeno-associated viral vectors. *Nat. Med.* **10**, 828–834 (2004).
56. G. A. Cox, N. M. Cole, K. Matsumura, S. F. Phelps, S. D. Hauschka, K. P. Campbell, J. A. Faulkner, J. S. Chamberlain, Overexpression of dystrophin in transgenic *mdx* mice eliminates dystrophic symptoms without toxicity. *Nature* **364**, 725–729 (1993).
57. S. Q. Harper, M. A. Hauser, C. DelloRusso, D. Duan, R. W. Crawford, S. F. Phelps, H. A. Harper, A. S. Robinson, J. F. Engelhardt, S. V. Brooks, J. S. Chamberlain, Modular flexibility of dystrophin: Implications for gene therapy of Duchenne muscular dystrophy. *Nat. Med.* **8**, 253–261 (2002).
58. B. Bostick, Y. Yue, Y. Lai, C. Long, D. Li, D. Duan, Adeno-associated virus serotype-9 micro-dystrophin gene therapy ameliorates electrocardiographic abnormalities in *mdx* mice. *Hum. Gene Ther.* **19**, 851–856 (2008).
59. D. J. Burkin, G. Q. Wallace, D. J. Milner, E. J. Chaney, J. A. Mulligan, S. J. Kaufman, Transgenic expression of $\alpha 7 \beta 1$ integrin maintains muscle integrity, increases regenerative capacity, promotes hypertrophy, and reduces cardiomyopathy in dystrophic mice. *Am. J. Pathol.* **166**, 253–263 (2005).
60. D. J. Burkin, G. Q. Wallace, K. J. Nicol, D. J. Kaufman, S. J. Kaufman, Enhanced expression of the $\alpha 7 \beta 1$ integrin reduces muscular dystrophy and restores viability in dystrophic mice. *J. Cell Biol.* **152**, 1207–1218 (2001).
61. N. Deconinck, J. Tinsley, F. De Backer, R. Fisher, D. Kahn, S. Phelps, K. Davies, J. M. Gillis, Expression of truncated utrophin leads to major functional improvements in dystrophin-deficient muscles of mice. *Nat. Med.* **3**, 1216–1221 (1997).
62. M. Wehling, M. J. Spencer, J. G. Tidball, A nitric oxide synthase transgene ameliorates muscular dystrophy in *mdx* mice. *J. Cell Biol.* **155**, 123–131 (2001).
63. M. Wehling-Henricks, M. C. Jordan, K. P. Roos, B. Deng, J. G. Tidball, Cardiomyopathy in dystrophin-deficient hearts is prevented by expression of a neuronal nitric oxide synthase transgene in the myocardium. *Hum. Mol. Genet.* **14**, 1921–1933 (2005).
64. N. Stupka, D. R. Plant, J. D. Schertzer, T. M. Emerson, R. Bassel-Duby, E. N. Olson, G. S. Lynch, Activated calcineurin ameliorates contraction-induced injury to skeletal muscles of *mdx* dystrophic mice. *J. Physiol.* **575**, 645–656 (2006).

65. S. Bogdanovich, T. O. Krag, E. R. Barton, L. D. Morris, L. A. Whittemore, R. S. Ahima, T. S. Khurana, Functional improvement of dystrophic muscle by myostatin blockade. *Nature* **420**, 418–421 (2002).
66. K. R. Wagner, A. C. McPherron, N. Winik, S. J. Lee, Loss of myostatin attenuates severity of muscular dystrophy in *mdx* mice. *Ann. Neurol.* **52**, 832–836 (2002).
67. P. Kronqvist, N. Kawaguchi, R. Albrechtsen, X. Xu, H. D. Schröder, B. Moghadaszadeh, F. C. Nielsen, C. Fröhlich, E. Engvall, U. M. Wewer, ADAM12 alleviates the skeletal muscle pathology in *mdx* dystrophic mice. *Am. J. Pathol.* **161**, 1535–1540 (2002).
68. S. Acharyya, S. A. Villalta, N. Bakkar, T. Bupha-Intr, P. M. Janssen, M. Carathers, Z. W. Li, A. A. Beg, S. Ghosh, Z. Sahenk, M. Weinstein, K. L. Gardner, J. A. Rafael-Fortney, M. Karin, J. G. Tidball, A. S. Baldwin, D. C. Guttridge, Interplay of IKK/NF- κ B signaling in macrophages and myofibers promotes muscle degeneration in Duchenne muscular dystrophy. *J. Clin. Invest.* **117**, 889–901 (2007).
69. A. Goyenvalle, A. Vulin, F. Fougereuse, F. Leturcq, J. C. Kaplan, L. Garcia, O. Danos, Rescue of dystrophic muscle through U7 snRNA-mediated exon skipping. *Science* **306**, 1796–1799 (2004).
70. Q. L. Lu, C. J. Mann, F. Lou, G. Bou-Gharios, G. E. Morris, S. A. Xue, S. Fletcher, T. A. Partridge, S. D. Wilton, Functional amounts of dystrophin produced by skipping the mutated exon in the *mdx* dystrophic mouse. *Nat. Med.* **9**, 1009–1014 (2003).
71. J. Alter, F. Lou, A. Rabinowitz, H. Yin, J. Rosenfeld, S. D. Wilton, T. A. Partridge, Q. L. Lu, Systemic delivery of morpholino oligonucleotide restores dystrophin expression body-wide and improves dystrophic pathology. *Nat. Med.* **12**, 175–177 (2006).
72. S. Fletcher, K. Honeyman, A. M. Fall, P. L. Harding, R. D. Johnsen, J. P. Steinhaus, H. M. Moulton, P. L. Iversen, S. D. Wilton, Morpholino oligomer-mediated exon skipping averts the onset of dystrophic pathology in the *mdx* mouse. *Mol. Ther.* **15**, 1587–1592 (2007).
73. F. Muntoni, D. Wells, Genetic treatments in muscular dystrophies. *Curr. Opin. Neurol.* **20**, 590–594 (2007).
74. M. J. Wood, M. J. Gait, H. Yin, RNA-targeted splice-correction therapy for neuromuscular disease. *Brain* **133**, 957–972 (2010).
75. E. M. Welch, E. R. Barton, J. Zhuo, Y. Tomizawa, W. J. Friesen, P. Trifillis, S. Paushkin, M. Patel, C. R. Trotta, S. Hwang, R. G. Wilde, G. Karp, J. Takasugi, G. Chen, S. Jones, H. Ren, Y. C. Moon, D. Corson, A. A. Turpoff, J. A. Campbell, M. M. Conn, A. Khan, N. G. Almstead, J. Hedrick, A. Mollin, N. Risher, M. Weetall, S. Yeh, A. A. Branstrom, J. M. Colacino, J. Babiak, W. D. Ju, S. Hirawat, V. J. Northcutt, L. L. Miller, P. Spatrick, F. He, M. Kawana, H. Feng, A. Jacobson, S. W. Peltz, H. L. Sweeney, PTC124 targets genetic disorders caused by nonsense mutations. *Nature* **447**, 87–91 (2007).
76. E. R. Barton-Davis, L. Cordier, D. I. Shoturma, S. E. Leland, H. L. Sweeney, Aminoglycoside antibiotics restore dystrophin function to skeletal muscles of *mdx* mice. *J. Clin. Invest.* **104**, 375–381 (1999).
77. Y. Hagiwara, Y. Mizuno, M. Takemitsu, T. Matsuzaki, I. Nonaka, E. Ozawa, Dystrophin-positive muscle fibers following C2 myoblast transplantation into *mdx* nude mice. *Acta Neuropathol.* **90**, 592–600 (1995).
78. J. Huard, G. Acsadi, A. Jani, B. Massie, G. Karpati, Gene transfer into skeletal muscles by isogenic myoblasts. *Hum. Gene Ther.* **5**, 949–958 (1994).
79. G. M. Mythe, Y. Fan, M. D. Grounds, Enhanced migration and fusion of donor myoblasts in dystrophic and normal host muscle. *Muscle Nerve* **23**, 560–574 (2000).
80. S. Corti, S. Strazzer, R. Del Bo, S. Salani, P. Bossolasco, F. Fortunato, F. Locatelli, D. Soligo, M. Moggi, P. Ciscato, A. Prella, C. Borsotti, N. Bresolin, G. Scarlato, G. P. Comi, A subpopulation of murine bone marrow cells fully differentiates along the myogenic pathway and participates in muscle repair in the *mdx* dystrophic mouse. *Exp. Cell Res.* **277**, 74–85 (2002).
81. Y. Torrente, M. Belicchi, M. Sampaolese, F. Pisati, M. Meregalli, G. D'Antona, R. Tonlorenzi, L. Porretti, M. Gavina, K. Mamchaoui, M. A. Pellegrino, D. Furling, V. Mouly, G. S. Butler-Browne, R. Bottinelli, G. Cossu, N. Bresolin, Human circulating AC133⁺ stem cells restore dystrophin expression and ameliorate function in dystrophic skeletal muscle. *J. Clin. Invest.* **114**, 182–195 (2004).
82. E. Gussoni, Y. Soneoka, C. D. Strickland, E. A. Buzney, M. K. Khan, A. F. Flint, L. M. Kunkel, R. C. Mulligan, Dystrophin expression in the *mdx* mouse restored by stem cell transplantation. *Nature* **401**, 390–394 (1999).
83. H. G. Radley, A. De Luca, G. S. Lynch, M. D. Grounds, Duchenne muscular dystrophy: Focus on pharmaceutical and nutritional interventions. *Int. J. Biochem. Cell Biol.* **39**, 469–477 (2007).
84. U. T. Ruegg, V. Nicolas-Metral, C. Challet, K. Bernard-Helary, O. M. Dorchies, S. Wagner, T. M. Buetler, Pharmacological control of cellular calcium handling in dystrophic skeletal muscle. *Neuromuscul. Disord.* **12** (Suppl. 1), S155–S161 (2002).
85. D. M. Escolar, C. G. Scacheri, Pharmacologic and genetic therapy for childhood muscular dystrophies. *Curr. Neurol. Neurosci. Rep.* **1**, 168–174 (2001).
86. A. E. Deconinck, J. A. Rafael, J. A. Skinner, S. C. Brown, A. C. Potter, L. Metzinger, D. J. Watt, J. G. Dickson, J. M. Tinsley, K. E. Davies, Utrophin-dystrophin-deficient mice as a model for Duchenne muscular dystrophy. *Cell* **90**, 717–727 (1997).
87. J. E. Rooney, J. V. Welsler, M. A. Dechert, N. L. Flintoff-Dye, S. J. Kaufman, D. J. Burkin, Severe muscular dystrophy in mice that lack dystrophin and $\alpha 7$ integrin. *J. Cell Sci.* **119**, 2185–2195 (2006).
88. R. M. Grady, R. W. Grange, K. S. Lau, M. M. Maimone, M. C. Nichol, J. T. Stull, J. R. Sanes, Role for α -dystrobrevin in the pathogenesis of dystrophin-dependent muscular dystrophies. *Nat. Cell Biol.* **1**, 215–220 (1999).
89. L. A. Megency, B. Kablar, R. L. Perry, C. Ying, L. May, M. A. Rudnicki, Severe cardiomyopathy in mice lacking dystrophin and MyoD. *Proc. Natl. Acad. Sci. U.S.A.* **96**, 220–225 (1999).
90. C. A. Sewry, K. Matsumura, K. P. Campbell, V. Dubowitz, Expression of dystrophin-associated glycoproteins and utrophin in carriers of Duchenne muscular dystrophy. *Neuromuscul. Disord.* **4**, 401–409 (1994).
91. M. Bakay, P. Zhao, J. Chen, E. P. Hoffman, A web-accessible complete transcriptome of normal human and DMD muscle. *Neuromuscul. Disord.* **12** (Suppl. 1), S125–S141 (2002).
92. J. H. Yoon, K. Chandrasekharan, R. Xu, M. Glass, N. Singhal, P. T. Martin, The synaptic CT carbohydrate modulates binding and expression of extracellular matrix proteins in skeletal muscle: Partial dependence on utrophin. *Mol. Cell. Neurosci.* **41**, 448–463 (2009).
93. A. Varki, Nothing in glycobiology makes sense, except in the light of evolution. *Cell* **126**, 841–845 (2006).
94. N. M. Varki, A. Varki, Diversity in cell surface sialic acid presentations: Implications for biology and disease. *Lab. Invest.* **87**, 851–857 (2007).
95. T. Kawano, S. Koyama, H. Takematsu, Y. Kozutsumi, H. Kawasaki, S. Kawashima, T. Kawasaki, A. Suzuki, Molecular cloning of cytidine monophospho-N-acetylneuraminic acid hydroxylase. Regulation of species- and tissue-specific expression of N-glycolylneuraminic acid. *J. Biol. Chem.* **270**, 16458–16463 (1995).
96. L. Shaw, P. Schneckeburger, J. Carlsen, K. Christiansen, R. Schauer, Mouse liver cytidine-5'-monophosphate-N-acetylneuraminic acid hydroxylase. Catalytic function and regulation. *Eur. J. Biochem.* **206**, 269–277 (1992).
97. N. J. Sharp, J. N. Kornegay, S. D. Van Camp, M. H. Herbstreith, S. L. Secore, S. Kettle, W. Y. Hung, C. D. Constantinou, M. J. Dykstra, A. D. Roses, R. J. Bartlett, An error in dystrophin mRNA processing in golden retriever muscular dystrophy, an animal homologue of Duchenne muscular dystrophy. *Genomics* **13**, 115–121 (1992).
98. J. N. Kornegay, S. M. Tuler, D. M. Miller, D. C. Levesque, Muscular dystrophy in a litter of golden retriever dogs. *Muscle Nerve* **11**, 1056–1064 (1988).
99. K. Nakamura, T. Ariga, T. Yahagi, T. Miyatake, A. Suzuki, T. Yamakawa, Interspecies comparison of muscle gangliosides by two-dimensional thin-layer chromatography. *J. Biochem.* **94**, 1359–1365 (1983).
100. P. Tangvoranuntakul, P. Gagneux, S. Diaz, M. Bardor, N. Varki, A. Varki, E. Muchmore, Human uptake and incorporation of an immunogenic nonhuman dietary sialic acid. *Proc. Natl. Acad. Sci. U.S.A.* **100**, 12045–12050 (2003).
101. H. H. Chou, H. Takematsu, S. Diaz, J. Iber, E. Nickerson, K. L. Wright, E. A. Muchmore, D. L. Nelson, S. T. Warren, A. Varki, A mutation in human CMP-sialic acid hydroxylase occurred after the Homo-Pan divergence. *Proc. Natl. Acad. Sci. U.S.A.* **95**, 11751–11756 (1998).
102. M. Bardor, D. H. Nguyen, S. Diaz, A. Varki, Mechanism of uptake and incorporation of the non-human sialic acid N-glycolylneuraminic acid into human cells. *J. Biol. Chem.* **280**, 4228–4237 (2005).
103. V. Padler-Karavani, H. Yu, H. Cao, H. Chokhawala, F. Karp, N. Varki, X. Chen, A. Varki, Diversity in specificity, abundance, and composition of anti-Neu5Gc antibodies in normal humans: Potential implications for disease. *Glycobiology* **18**, 818–830 (2008).
104. D. H. Nguyen, P. Tangvoranuntakul, A. Varki, Effects of natural human antibodies against a nonhuman sialic acid that metabolically incorporates into activated and malignant immune cells. *J. Immunol.* **175**, 228–236 (2005).
105. M. Hedlund, V. Padler-Karavani, N. M. Varki, A. Varki, Evidence for a human-specific mechanism for diet and antibody-mediated inflammation in carcinoma progression. *Proc. Natl. Acad. Sci. U.S.A.* **105**, 18936–18941 (2008).
106. E. Byres, A. W. Paton, J. C. Paton, J. C. Löfling, D. F. Smith, M. C. Wilce, U. M. Talbot, D. C. Chong, H. Yu, S. Huang, X. Chen, N. M. Varki, A. Varki, J. Rossjohn, T. Beddoe, Incorporation of a non-human glycan mediates human susceptibility to a bacterial toxin. *Nature* **456**, 648–652 (2008).
107. R. Xu, K. Chandrasekharan, J. H. Yoon, M. Camboni, P. T. Martin, Overexpression of the cytotoxic T cell (CT) carbohydrate inhibits muscular dystrophy in the *dy^w* mouse model of congenital muscular dystrophy 1A. *Am. J. Pathol.* **171**, 181–199 (2007).
108. R. Xu, S. DeVries, M. Camboni, P. T. Martin, Overexpression of *Galg2* reduces dystrophic pathology in the skeletal muscles of α sarcoglycan-deficient mice. *Am. J. Pathol.* **175**, 235–247 (2009).
109. M. Hedlund, P. Tangvoranuntakul, H. Takematsu, J. M. Long, G. D. Housley, Y. Kozutsumi, A. Suzuki, A. Wynshaw-Boris, A. F. Ryan, R. L. Gallo, N. Varki, A. Varki, N-glycolylneuraminic acid deficiency in mice: Implications for human biology and evolution. *Mol. Cell. Biol.* **27**, 4340–4346 (2007).
110. S. L. Diaz, V. Padler-Karavani, D. Ghaderi, N. Hurtado-Ziola, H. Yu, X. Chen, E. C. Brinkman-Van der Linden, A. Varki, N. M. Varki, Sensitive and specific detection of the non-human sialic acid N-glycolylneuraminic acid in human tissues and biotherapeutic products. *PLoS One* **4**, e4241 (2009).
111. P. Pacher, T. Nagayama, P. Mukhopadhyay, S. Bátkai, D. A. Kass, Measurement of cardiac function using pressure-volume conductance catheter technique in mice and rats. *Nat. Protoc.* **3**, 1422–1434 (2008).

112. A. Varki, Glycan-based interactions involving vertebrate sialic-acid-recognizing proteins. *Nature* **446**, 1023–1029 (2007).
113. T. Sasaki, H. Yamada, K. Matsumura, T. Shimizu, A. Kobata, T. Endo, Detection of O-mannosyl glycans in rabbit skeletal muscle α -dystroglycan. *Biochim. Biophys. Acta* **1425**, 599–606 (1998).
114. R. Xu, M. Camboni, P. T. Martin, Postnatal overexpression of the CT GalNAc transferase inhibits muscular dystrophy in mdx mice without altering muscle growth or neuromuscular development: Evidence for a utrophin-independent mechanism. *Neuromuscul. Disord.* **17**, 209–220 (2007).
115. J. M. Ervasti, K. J. Sonnemann, Biology of the striated muscle dystrophin–glycoprotein complex. *Int. Rev. Cytol.* **265**, 191–225 (2008).
116. R. C. Hirst, K. J. McCullagh, K. E. Davies, Utrophin upregulation in Duchenne muscular dystrophy. *Acta Myol.* **24**, 209–216 (2005).
117. R. M. Grady, H. Teng, M. C. Nichol, J. C. Cunningham, R. S. Wilkinson, J. R. Sanes, Skeletal and cardiac myopathies in mice lacking utrophin and dystrophin: A model for Duchenne muscular dystrophy. *Cell* **90**, 729–738 (1997).
118. L. Zhou, J. A. Rafael-Fortney, P. Huang, X. S. Zhao, G. Cheng, X. Zhou, H. J. Kaminski, L. Liu, R. M. Ransohoff, Haploinsufficiency of utrophin gene worsens skeletal muscle inflammation and fibrosis in mdx mice. *J. Neurol. Sci.* **264**, 106–111 (2008).
119. J. Peng, K. Raddatz, J. D. Molkentin, Y. Wu, S. Labeit, H. Granzier, M. Gotthardt, Cardiac hypertrophy and reduced contractility in hearts deficient in the titin kinase region. *Circulation* **115**, 743–751 (2007).
120. M. J. Spencer, J. G. Tidball, Do immune cells promote the pathology of dystrophin-deficient myopathies? *Neuromuscul. Disord.* **11**, 556–564 (2001).
121. J. G. Tidball, S. A. Villalta, Regulatory interactions between muscle and the immune system during muscle regeneration. *Am. J. Physiol. Regul. Integr. Comp. Physiol.* **298**, R1173–R1187 (2010).
122. J. G. Tidball, Inflammatory cell response to acute muscle injury. *Med. Sci. Sports Exerc.* **27**, 1022–1032 (1995).
123. C. M. Wang, S. Devries, M. Camboni, M. Glass, P. T. Martin, Immunization with the SDPM1 peptide lowers amyloid plaque burden and improves cognitive function in the APP^{swe}PSEN1 (A246E) transgenic mouse model of Alzheimer's disease. *Neurobiol. Dis.*, in press.
124. E. R. Podack, V. Deyev, M. Shiratsuchi, Pore formers of the immune system. *Adv. Exp. Med. Biol.* **598**, 325–341 (2007).
125. M. J. Martin, J. C. Rayner, P. Gagneux, J. W. Barnwell, A. Varki, Evolution of human-chimpanzee differences in malaria susceptibility: Relationship to human genetic loss of N-glycolylneuraminic acid. *Proc. Natl. Acad. Sci. U.S.A.* **102**, 12819–12824 (2005).
126. A. G. Engel, G. Biesecker, Complement activation in muscle fiber necrosis: Demonstration of the membrane attack complex of complement in necrotic fibers. *Ann. Neurol.* **12**, 289–296 (1982).
127. G. Karpati, S. Carpenter, "Killer" cell activity in Duchenne muscular dystrophy. *Neurology* **36**, 135–137 (1986).
128. B. Xia, P. T. Martin, Modulation of agrin binding and activity by the CT and related carbohydrate antigens. *Mol. Cell. Neurosci.* **19**, 539–551 (2002).
129. P. M. Janssen, N. Hiranandani, T. A. Mays, J. A. Rafael-Fortney, Utrophin deficiency worsens cardiac contractile dysfunction present in dystrophin-deficient mdx mice. *Am. J. Physiol. Heart Circ. Physiol.* **289**, H2373–H2378 (2005).
130. K. Hoyte, V. Jayasinha, B. Xia, P. T. Martin, Transgenic overexpression of dystroglycan does not inhibit muscular dystrophy in mdx mice. *Am. J. Pathol.* **164**, 711–718 (2004).
131. V. Jayasinha, H. H. Nguyen, B. Xia, A. Kammesheidt, K. Hoyte, P. T. Martin, Inhibition of dystroglycan cleavage causes muscular dystrophy in transgenic mice. *Neuromuscul. Disord.* **13**, 365–375 (2003).
132. E. C. Brinkman-Van der Linden, A. Varki, New aspects of siglec binding specificities, including the significance of fucosylation and of the sialyl-Tn epitope. *J. Biol. Chem.* **275**, 8625–8632 (2000).
133. K. J. Livak, T. D. Schmittgen, Analysis of relative gene expression data using real-time quantitative PCR and the $2^{-\Delta\Delta CT}$ method. *Methods* **25**, 402–408 (2001).
134. M. A. Kutzler, C. Cao, Y. Bai, H. Dong, P. Y. Choe, V. Saulino, L. McLaughlin, A. Whelan, A. Y. Choo, D. B. Weiner, K. E. Ugen, Mapping of immune responses following wild-type and mutant A β 42 plasmid or peptide vaccination in different mouse haplotypes and HLA class II transgenic mice. *Vaccine* **24**, 4630–4639 (2006).
135. B. Xia, K. Hoyte, A. Kammesheidt, T. Deerinck, M. Ellisman, P. T. Martin, Overexpression of the CT GalNAc transferase in skeletal muscle alters myofiber growth, neuromuscular structure, and laminin expression. *Dev. Biol.* **242**, 58–73 (2002).
136. **Acknowledgments:** We thank J. Mendell (Nationwide Children's Hospital/Ohio State University) and Z. Sahenk (Nationwide Children's Hospital/Ohio State University) for help in analyzing and interpreting staining of clinical muscle samples; C.-M. Wang, C. Gregg, M. Glass, J. Saik, E. Ogelsbay, R. Xu, A. Birdi, B. Canan, K. Quinter, B. Xia, L. Guo, S. Diaz, and S. Lewis for technical support; H. Auer and the Gene Microarray Core at Nationwide Children's Hospital for assistance in microarray studies; J. Mendell (Nationwide Children's Hospital/Ohio State University) for critically reading the manuscript; D. Guttridge (Ohio State University) for assistance in experimental design; and M. Periasamy (Ohio State University) for providing rabbit polyclonal antiserum specific to Serca2a. **Funding:** This work was supported by NIH grants R01 AR050202 and R01 AR049722 (P.T.M.), R01 HL083957 (P.M.L.J.), and R01GM32373 and R01CA38701 (A.V.) and a collaborative grant from Ohio State University Medical School and Nationwide Children's Hospital (P.T.M. and P.M.L.J.). PAA-biotinylated glycans were obtained from the Consortium for Functional Glycomics (Core D), which is supported by National Institute of General Medical Sciences grant GM62116 (J. Paulson, principal investigator). **Author contributions:** P.T.M. designed the study, analyzed all data, and wrote the paper, with editorial input from A.V., K.C., and P.M.L.J. P.T.M. and K.C. analyzed all cellular and molecular data. K.C. did most of the experiments, with significant assistance from J.H.Y., M.C., and S.d.V. J.H.Y. did all ECM-binding experiments, whereas M.C. and S.d.V. did most assessments of muscle histopathology. A.V. made the *Cmah*^{-/-} mice, provided and characterized the Neu5Gc-specific reagents, and analyzed sialic acid content and profiles. P.M.L.J. and Y.X. performed and analyzed all cardiac and skeletal muscle physiology studies. **Competing interests:** A.V. is a board member and co-founder of Sialix Inc. (formerly Gc-Free Inc.), a biotech company focused on developing therapeutics related to sialic acid. None of the other authors have any competing interests to declare. **Accession numbers:** Array data are available from the Gene Expression Omnibus repository (<http://www.ncbi.nlm.nih.gov/geo>) under accession numbers GSM413160 to GSM413182.

Submitted 1 December 2009

Accepted 9 July 2010

Published 28 July 2010

10.1126/scitranslmed.3000692

Citation: K. Chandrasekharan, J. H. Yoon, Y. Xu, S. deVries, M. Camboni, P. M. L. Janssen, A. Varki, P. T. Martin, A human-specific deletion in mouse *Cmah* increases disease severity in the mdx model of Duchenne muscular dystrophy. *Sci. Transl. Med.* **2**, 42ra54 (2010).

Supplementary Materials for

A Human-Specific Deletion in Mouse *Cmah* Increases Disease Severity in the mdx Model of Duchenne Muscular Dystrophy

Kumaran Chandrasekharan, Jung Hae Yoon, Ying Xu, Sarah deVries, Marybeth Camboni, Paulus M. L. Janssen, Ajit Varki, Paul T. Martin*

*To whom correspondence should be addressed. E-mail: paul.martin@nationwidechildrens.org

Published 28 July 2010, *Sci. Transl. Med.* **2**, 42ra54 (2010)
DOI: 10.1126/scitranslmed.3000692

The PDF file includes:

- Fig. S1. Characterization of Neu5Gc and sialic acid expression in dystrophic and normal mice and humans.
- Fig. S2. Analysis of histopathology and muscle features in *Cmah*-deficient mdx animals.
- Fig. S3. Characterization of materials used for binding assays and serum titers.
- Fig. S4. Binding of recombinant agrins and laminins to α DG glycoforms and to Neu5Gc and Neu5Ac sialylglycoconjugates.
- Fig. S5. Staining of heart and skeletal muscles with antibody to activated C5b-9 complement.
- Fig. S6. Coexpression of activated (C5b-9) complement with embryonic myosin, Neu5Gc, and endogenous mouse antibody in *Cmah*^{-/-}mdx muscle.
- Table S1. TaqMan gene expression assays used for real-time PCR.

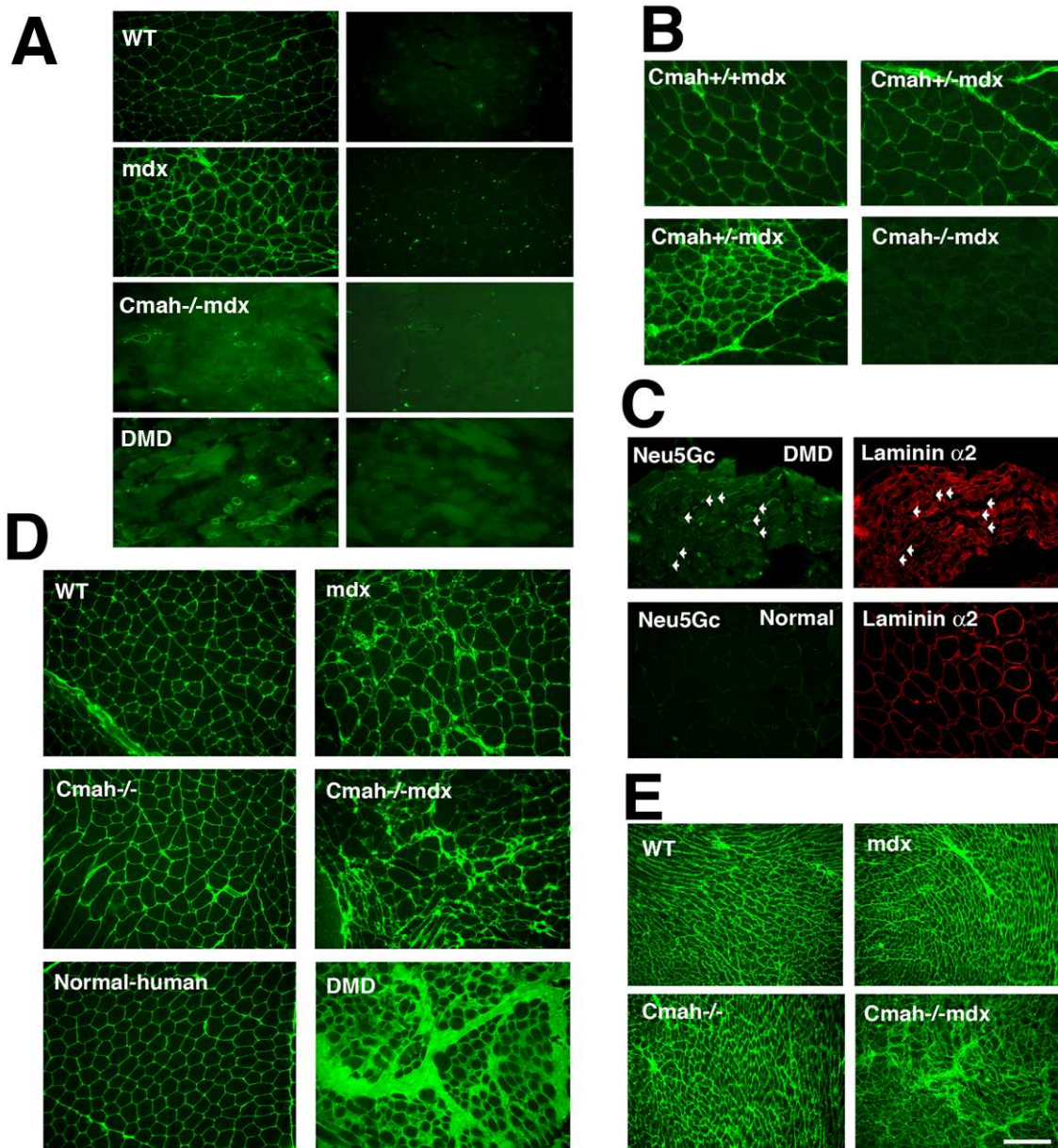


Figure S1. Characterization of Neu5Gc and sialic acid expression in dystrophic and normal mice and humans. (A) Control non-immune chicken IgY antibody (right panels) is compared to affinity purified, mono-specific, anti-Neu5Gc chicken IgY (left panels) for immunostaining of skeletal muscles, where conditions were otherwise identical. Skeletal muscles where Neu5Gc staining was positive on myofibers (Wild type (WT), mdx, *Cmah*^{-/-}mdx and human Duchenne muscular dystrophy (DMD)) showed background staining of mononuclear cells but no staining of myofibers with non-immune antibody. (B) mdx mice containing two wild type alleles of mouse *Cmah* (*Cmah*^{+/+}mdx) or one wild type and one human-like deleted allele (*Cmah*^{+/-}mdx) both showed high Neu5Gc expression along the sarcolemmal membrane of skeletal myofibers. In regenerating muscles, Neu5Gc expression was increased relative to non-dystrophic myofibers. Most regions in *Cmah*^{-/-}mdx muscle did not express Neu5Gc. (C) Regenerating myofibers in skeletal muscle biopsies taken from patients with Duchenne muscular dystrophy showed significant Neu5Gc expression (arrows) in some myofibers prior to expression of laminin α 2 (merosin). (D) Wild type (WT), *Cmah*-deficient (*Cmah*^{-/-}), dystrophin-deficient (mdx), *Cmah*^{-/-}mdx, normal human, and Duchenne muscular dystrophy (DMD) skeletal muscles all showed high staining with *Maackia ameurensis* agglutinin (MAA), a lectin that recognizes both Neu5Gc and Neu5Ac α 2-3-linked sialic acids. (E) WT, *Cmah*^{-/-}, mdx, and *Cmah*^{-/-}mdx hearts all showed high MAA staining of cardiomyocytes. Bar is 75 μ m in B and D, 100 μ m in A and C, and 200 μ m in E.

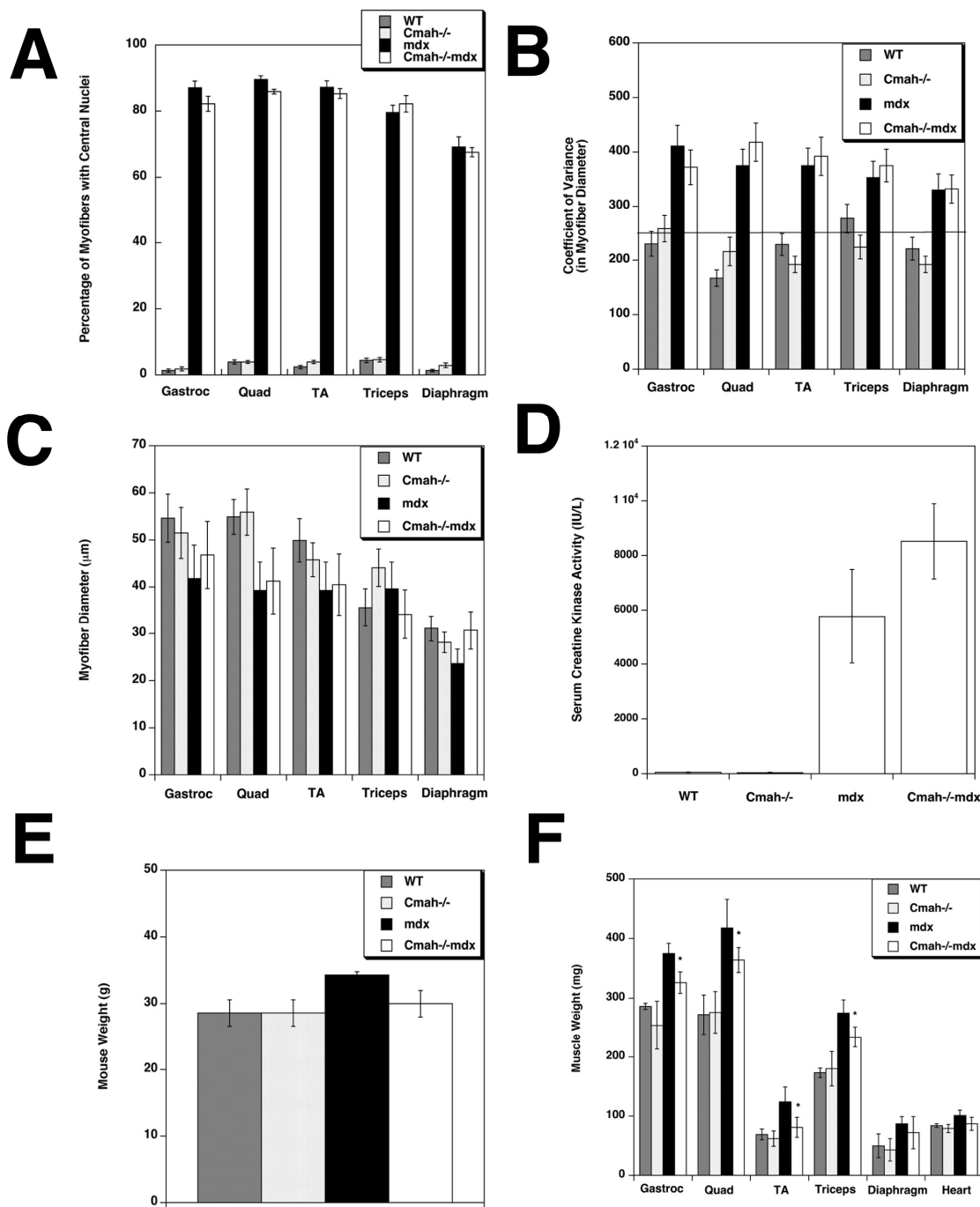
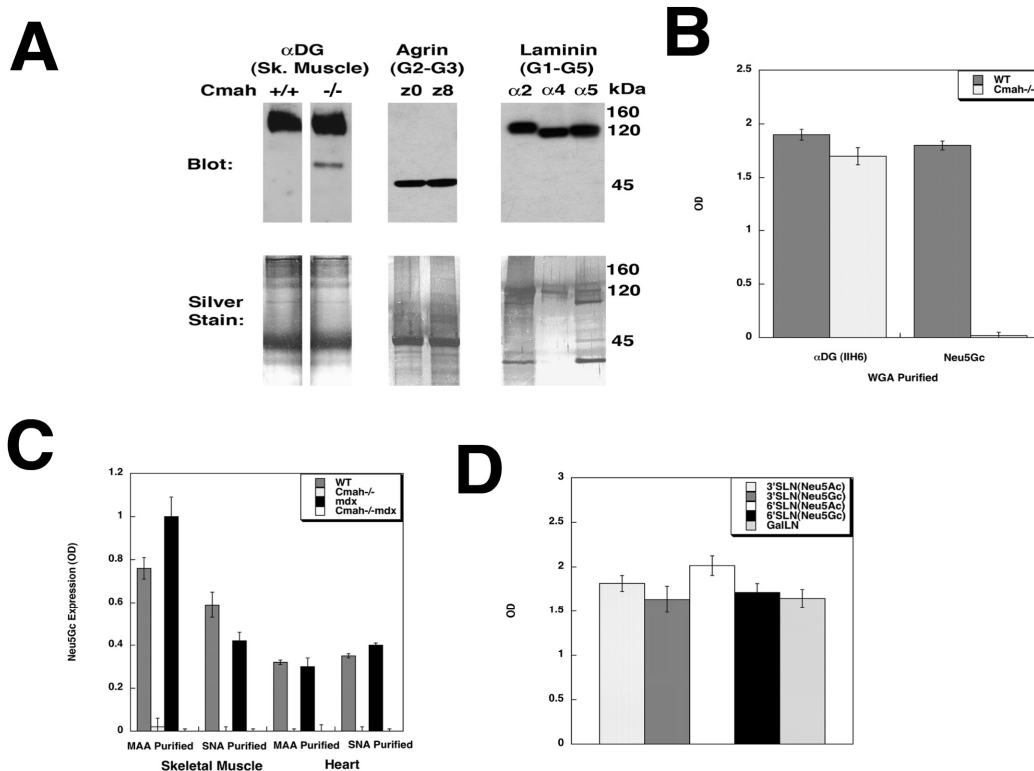
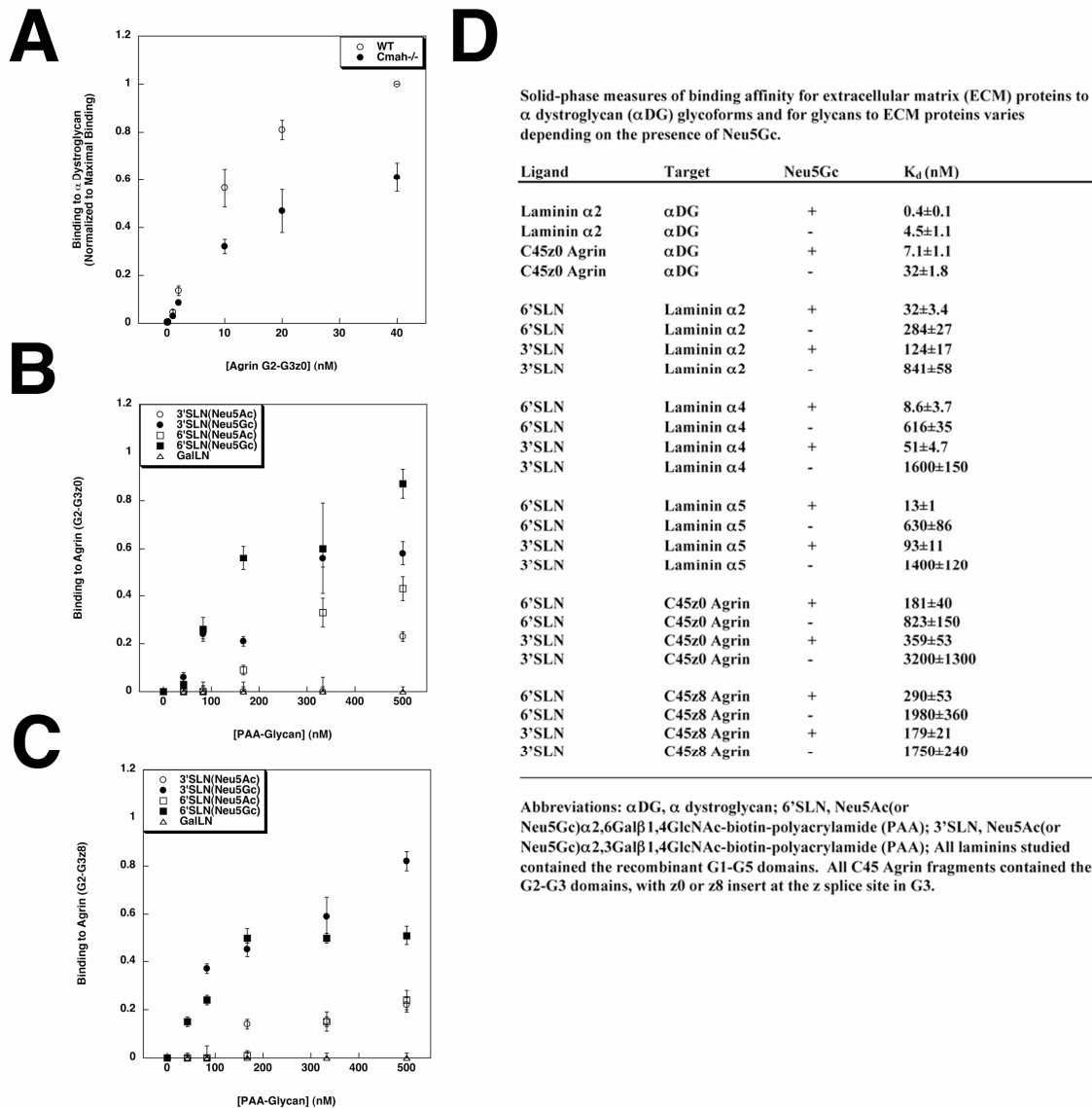


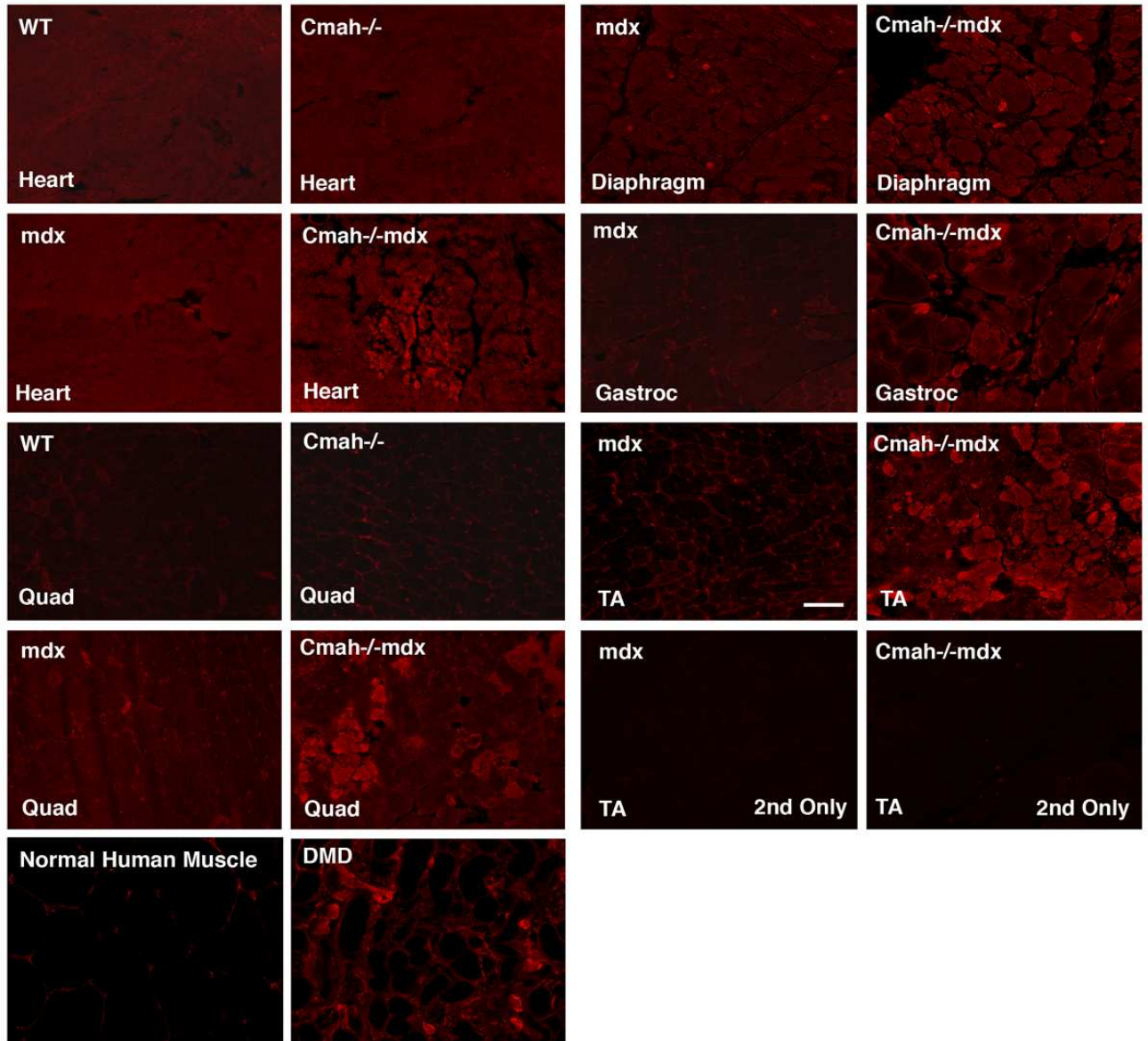
Fig. S2. Analysis of histopathology and muscle features in *Cmah*-deficient *mdx* animals. (A-D) Histopathology measures that are normally high in *mdx* mice were equally high or higher in *Cmah*^{-/-}*mdx* mice. (A) Percentages of skeletal myofibers with central nuclei were increased equally in *mdx* and *Cmah*^{-/-}*mdx* muscles. (B) Coefficient of variance in skeletal myofiber diameter exceeded the level considered to reflect dystrophic muscles (>250) in all *mdx* and *Cmah*^{-/-}*mdx* muscles. (C) Measures of average myofiber diameter. (D) Serum creatine kinase activity was elevated in both *mdx* and *Cmah*^{-/-}*mdx* muscles. (E) *mdx* mice and (F) *mdx* skeletal muscles were increased in weight relative to WT, while some *Cmah*^{-/-}*mdx* muscles were decreased in weight relative to *mdx*. Measures for A-C and E-F were taken at 5 months of age. Measures for D were taken at 2 months of age. Errors are SEM for n=6 (A-C, F) or n=6-12 (D-E) per condition. *P<0.05



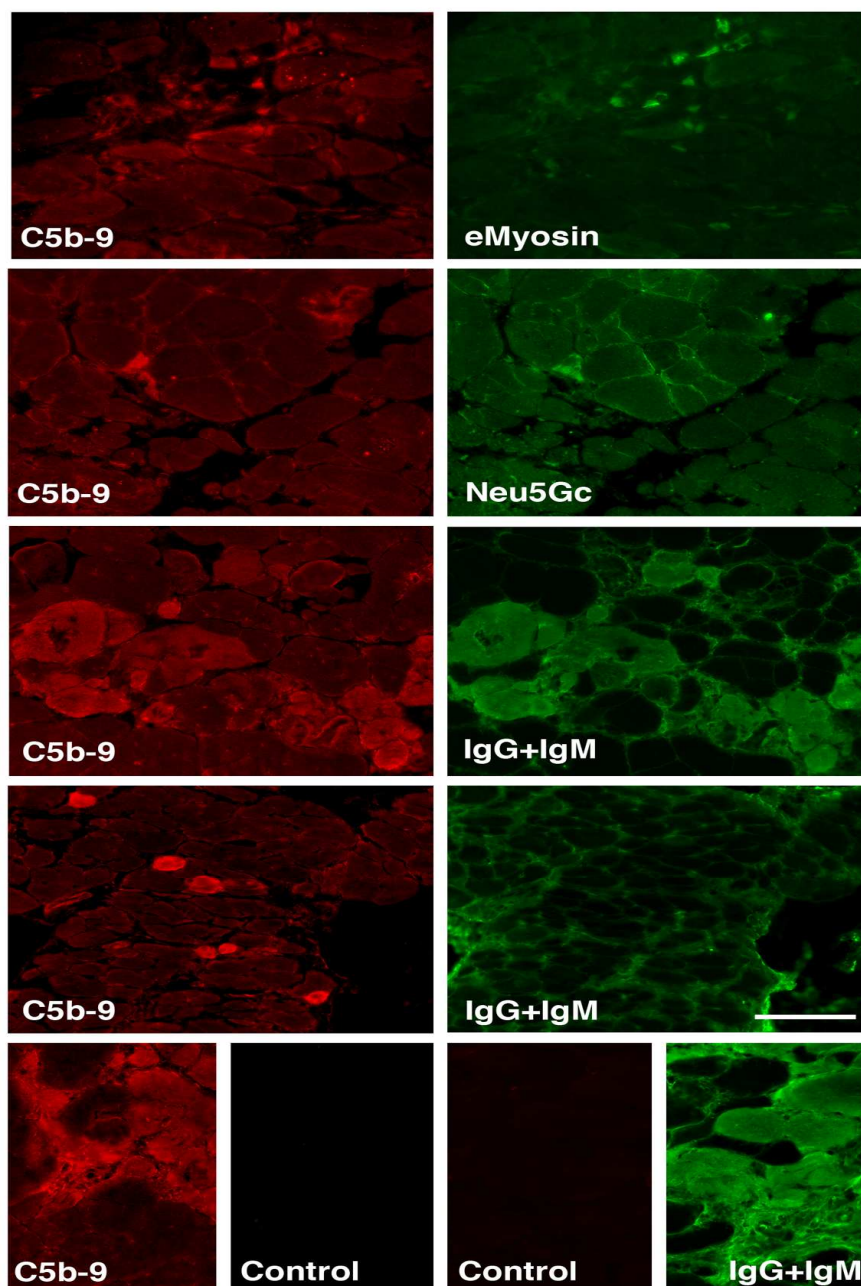
Supplemental Figure 3. Characterization of materials used for binding assays and serum titers. α/β dystroglycan complex was purified by WGA lectin chromatography from skeletal muscles of wild type (*Cmah*^{+/+}) or *Cmah*^{-/-} mice. Both α (160kDa) and β (43kDa) dystroglycan, which were evident by immunoblot (α DG blot with IIH6 is shown) and by silver stain. Note that α DG is more difficult to visualize than β DG by silver stain due to its very high level of glycosylation. Recombinant FLAG-tagged secreted forms of the G1-G5 domains of laminin α 2, α 4, or α 5, or the G2-G3 domains of the muscle splice form (z0) or the neural splice form (z8) of agrin were purified from transfected HEK293T cells with anti-FLAG (M2) affinity chromatography. Proteins of the proper molecular weight were observed by immunoblot using anti-FLAG immunoblotting and by silver staining of SDS-PAGE gels. Several laminins (α 2 and α 5) contained additional proteolytic fragments of recombinant laminin protein. (B) α DG purified from WT skeletal muscle and from *Cmah*^{-/-} skeletal muscle were immobilized on ELISA plates for solid-phase binding assays. α DG antibody (IIH6) recognized α DG equally well from both mouse genotypes, while only WT α DG showed Neu5Gc expression. (C) *Maackia amurensis* agglutinin (MAA) and *Sambucus nigra* agglutinin (SNA) were used to purify α 2-3-linked and α 2-6-linked sialic acid-containing glycoproteins, respectively, from WT, *Cmah*^{-/-}, mdx, and *Cmah*^{-/-}mdx skeletal muscle and heart. Purified glycoproteins were immobilized on each well and Neu5Gc levels were measured by ELISA. Both WT and mdx skeletal muscle and heart expressed high levels of Neu5Gc, while *Cmah*^{-/-} and *Cmah*^{-/-}mdx did not express detectable levels. (D) PAA-glycan used to measure binding to laminin and agrin were immobilized on ELISA plates to verify that equivalent amounts of biotin signal were present in equivalent amounts of PAA-glycan used. Errors are SEM for n=6 (B, C and D) per condition.



Supplemental Figure 4. Binding of recombinant agrins and laminins to α DG glycoforms and to Neu5Gc and Neu5Ac sialylglycoconjugates. (A) Binding of C45z0 agrin, the predominant muscle agrin, was compared to α dystroglycan (α DG) purified from WT muscles, which contain Neu5Gc, and *Cmah*^{-/-}-muscles, which do not. Experiments were normalized (at 1) to maximal binding within the experiment. SF4B and C were done contemporaneously with experiments shown in Figs. 4B-D, and are normalized to maximal binding shown in those experiments. (B) Binding of Neu5Gc- and Neu5Ac-sialylglycoconjugates to C45z0 agrin. (C) Binding of Neu5Gc- and Neu5Ac-sialylglycoconjugates to C45z8 agrin. (D) Relative apparent binding affinities were calculated for solid-phase binding studies shown in Figs 4A-D and Supplemental Figs. 4A-C. +Neu5Gc samples contained mixture of Neu5Gc and Neu5Ac sialoglycoproteins from wild type muscle, while -Neu5Gc contained sialoglycoproteins isolated from *Cmah*^{-/-} muscle, which contained no detectable Neu5Gc (see S3B). Errors are SEM for n=6-12 per condition in A-D.



Supplemental Figure 5. Staining of heart and skeletal muscles with antibody to activated C5b-9 complement. 5mo heart or skeletal muscles were immunostained with an antibody to activated C5b-9 complement. Muscle cells in *Cmah-/-mdx* heart, quadriceps, gastrocnemius, diaphragm, and tibialis anterior showed elevated staining relative to *mdx*, while no wild type (WT) or *Cmah-/-* muscles showed any staining. Skeletal muscle (Quad) from a 2 year-old DMD patient showed high C5b-9 complement deposition on a subset of myofibers, while normal human skeletal muscle was not stained. Bar is 50 μ m.



Supplemental Figure 6. Coexpression of activated (C5b-9) complement with embryonic myosin, Neu5Gc, and endogenous mouse antibody in *Cmah*^{-/-}mdx muscle. Small regenerating muscles positive for embryonic myosin (eMyosin) or for Neu5Gc were sometimes co-stained for activated C5b-9 complement. Some large and small regenerating muscles with C5b-9 complement deposition also showed deposition of endogenous mouse antibody (IgG+IgM, third panels from top), but some muscles with C5b-9 deposition showed no co-staining for mouse antibody (fourth panels from top). Muscles stained for C5b-9 complement (red) showed no signal in the green channel if primary antibody for the co-stain was left out (control, left), and muscles stained for mouse IgG+IgM (green) showed no signal in the red channel if C5b-9 antibody was left out (control, right). Bar is 100 μ m.

Table S1. TaqMan gene expression assays used for real-time PCR.

Gene Name	Gene	Applied Biosystems
	Symbol	TaqMan Assay ID
Angiotensin II receptor, type 1a	Agtr1a	Mm00616371_m1
ANP, natriuretic peptide precursor type A	Nppa	Mm01255747_g1
ATPase, Ca ⁺⁺ transporting, cardiac muscle, slow twitch 2 (SERCA2)	Atp2a2	Mm01201431_m1
BNP, natriuretic peptide precursor type B	Nppb	Mm00435304_g1
Calcineurin B, type I	Ppp3r1	Mm00470484_m1
CD68 antigen	Cd68	Mm00839636_g1
Chemokine (C-C motif) ligand 2 (MCP-1)	Ccl2	Mm99999056_m1
Chemokine (C-C motif) ligand 3 (MIP1-a)	Ccl3	Mm99999057_m1
Chemokine (C-C motif) ligand 5 (RANTES)	Ccl5	Mm01302427_m1
Collagen, type I, alpha 1	Col1a1	Mm00801666_g1
Collagen, type III, alpha 1	Col3a1	Mm00802331_m1
Endothelin 1	Edn1	Mm00438656_m1
Interleukin 1 beta	Il1b	Mm00434228_m1
Interleukin 6	Il6	Mm01210733_m1
Tumor necrosis factor – α	Tnf	Mm99999068_m1
Dystrobrevin Alpha	Dtna	Mm00494555_m1
Utrophin	Utrn	Mm01168861_m1

Laminin Alpha 1	Lama1	Mm01226098_m1
Laminin Alpha2	Lama2	Mm01193202_m1
Laminin Alpha 4	Lama4	Mm01190521_m1
Laminin Alpha 5	Lama5	Mm01222011_m1
Procollagen IV a1	Col4a1	Mm00802340_m1
Procollagen IV a2	Col4a2	Mm01216800_m1
Sarcoglycan Alpha	Sgca	Mm00486068_m1
Sarcoglycan Beta	Sgcb	Mm00449389_m1
Sarcoglycan Delta	Sgcd	Mm00449392_m1
Sarcoglycan Gamma	Sgcg	Mm00488741_m1
Agrin	Agrn	Mm01545840_m1
Integrin Alpha 7	Itga7	Mm01160040_m1
Integrin Beta 1	Itgb1	Mm01253239_m1
Dystroglycan 1	Dag1	Mm00802400_m1
CD4	Cd4	Mm00442754_m1
CD8	Cd8	Mm01182108_m1
